Table I. Parameters Used in Extended-Hückel Calculations

	orbital	H_{ii}, eV	1	2	C_1[a]	C_2[a]
Nb	4d	-12.10	4.08	1.637	0.6404	0.5519
	5s	-10.10	1.89			
	5p	-6.86	1.85			
P	3s	-18.60	1.88			
	3p	-14.00	1.63			
S	3s	-20.00	2.12			
	3p	-13.30	1.83			

[a] Coefficients of the double-ζ expansion.

these and related syntheses are currently under investigation.

Acknowledgment. Douglas Keszler thanks J. Silvestre, C. Zheng, and R. Wheeler for helpful discussions. We are also grateful to three reviewers for a careful reading of the paper, pointing out several errors and omissions. Our work was generously supported by the National Science Foundation through Research Grants DM 8217722 to the Materials Science Center at Cornell University and Grant CHE 8406119.

Appendix

All calculations were performed with the extended Hückel method.[26] The parameters used for the Nb, P, and S orbitals are listed in Table I. A set of 28 or more k points was chosen to calculate average properties.[27]

Registry No. NbPS, 26153-57-1; NbPSe, 26134-84-9; TaPS, 26134-85-0; TaPSe, 104911-45-7.

(26) Hoffmann, R. *J. Chem. Phys.* **1963**, *39*, 1397.
(27) Pack, J. D.; Monkhorst, J. *Phys. Rev. B* **1977**, *16*, 1748.

Square Nets of Main Group Elements in Solid-State Materials

Wolfgang Tremel[1] and Roald Hoffmann*

Contribution from the Department of Chemistry and Materials Science Center, Cornell University, Ithaca, New York 14853. *Received May 29, 1986*

Abstract: The Cu_2Sb/ZrSiS/PbFCl structure type—ubiquitous, as the number of synonyms shows—may be derived conceptually from a layering of square nets of atoms. One group of phases can be described as MAB (M: large metal atom; A and B: main group elements). M and B atoms form associated square nets. They are separated by a 4^4 layer of A atoms which is twice as dense as the individual M and B layers. In the more covalent, metallic MAB phases the A···A contacts within the 4^4 layers—which are our prime focus of interest—indicate bonds of fractional order. For M = Ln, A = P, As, and B = S two sets of distorted structure types exist. In the GdPS and CeAsS structures the layers distort to form cis-trans poly-P or zigzag poly-As chains, respectively. The electronic structure of the MAB phases is constructed, and the distortion is traced to a band crossing at the Fermi level. The deformation—a second-order Jahn-Teller distortion in the solid state—is driven by the formation of an energy gap at the Fermi level. The relative electronegativity of the M and A atoms dictates whether the distorted or undistorted structure is preferred. A prerequisite for the distortion to occur is a separation of valence band and metal d block. The general distortion type square net → zigzag chain can also be found in other phases containing 4^4 nets of main group atoms. Further examples treated here are the distortion from the $ZrSi_2$ to the $CaSb_2$ type structures and a deformation type found in ATB_2 phases, exemplified by $SrZnBi_2$.

It is not easy to think about extended structures in the solid state. There is always arbitrariness in the description of crystal structures, because one may want to stress either the chemistry of physical properties of a material or emphasize the structural relationship to other compounds. Choices of vantage must be made. Taking "Schnering's spectacles" and discovering clusters in solid-state compounds[2] is one particularly nice way to visualize crystal structures. Another, more traditional concept in crystal chemistry describes structures in terms of coordination polyhedra.[3] These polyhedra may then be oriented in various ways and connected via corners, edges, or faces. An alternative approach considers structures as being built up from two-dimensional layer stackings. The resulting description based on closest packing is especially useful in cases where polyhedra are difficult to define. Still another concept describes crystal structures in terms of stacked layers, but focussing now on the atom connectivity. Many structure types can be covered by considering only square (4^4), triangular (3^6), hexagonal (6^3), or kagome (3636) networks, **1a-d**.[4]

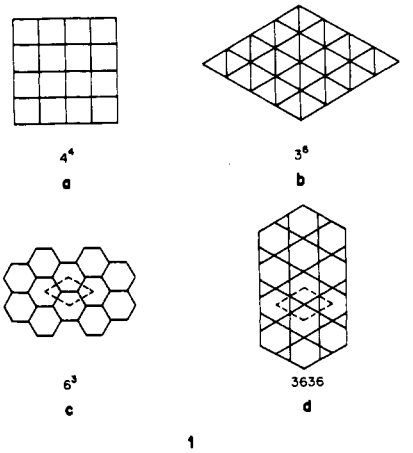

1

Each description may be mathematically well-defined but need not have a prior claim to general chemical or physical validity. A pragmatic perspective is best. To obtain a convenient description of solids we often switch from one description to another, according

(1) DAAD/NATO Postdoctoral Fellow 1984-1985. DFG Fellow 1985-1986. Present addresss: Anorganisch-Chemisches Institut der Universitüt, Correnstr. 36, D4400 Münster, F.R.G.
(2) (a) von Schnering, H.-G. *Angew. Chem.* **1983**, *93*, 44; *Angew. Chem., Int. Ed. Engl.* **1981**, *20*, 33. (b) Simon, A. *Angew. Chem.* **1981**, *93*, 23; *Angew. Chem., Int. Ed. Engl.* **1981**, *20*, 1.
(3) Gladyshevskii, E. I.; Grin', Yu. N. *Kristallografiya* **1981**, *26*, 1204; *Sov. Phys. Crystallogr.* **1981**, *26*, 683.
(4) (a) Pearson, W. B. *The Crystal Chemistry and Physics of Metals of Alloys*; Wiley: Interscience, 1972. (b) O'Keeffe, M.; Hyde, B. G. *Philos. Mag.* **1980**, *295A*, 38.
(5) (a) von Fedorov, E. *Z. Kristallogr. Mineral.* **1904**, *38*, 321. (b) von Fedorov, E. *Das Krystallreich, Tabellen zur krystallchemischen Analyse*, Petrograd, 1920.
(6) (a) Laves, F. *Theory of Alloy Phases*; Cleveland, Ohio, 1956; pp 124. (b) Laves, F. *Phase Stability in Metals and Alloys*; McGraw-Hill: New York, 1967; p 85.

0002-7863/87/1509-0124$01.50/0

to our immediate purpose and needs. Besides these geometrical and packing considerations the symmetry principle[5] as emphasized by Laves[6] and electron counting rules[7] have become empirical tools to explain composition and atomic arrangement of solid-state phases and to elucidate their structural principles. By using these instruments a hierarchic ordering of topologically related structures can be derived in the form of a family tree,[8] the parent structure on top being the aristotype and the subordinate structures the so-called hettotype structures.[9]

The same fragmentation and construction principles that apply to the geometrical description of extended structures may be invoked in analyzing their electronic structure. Sometimes one may want to emphasize clusters, and sometimes polyhedra or layers are more convenient building blocks. Stacking layers of certain connectivity is one architectonic principle we have found useful. In several other papers on the $ThCr_2Si_2$,[10] $CaBe_2Ge_2$,[11] and PbO[12] structures, and on the adsorption of small molecules on (100) metal surfaces,[13] we have analyzed the square net, which is also at the center of this paper.

The 4^4-square net **1a** is a common high symmetry structural pattern. The simplest three-dimensional structure based on it, the simple cubic or α-polonium structure, is not all that common. But intergrown,[14] slightly less symmetric three-dimensional arrays are common. These include UNi_2Si_3[15] and $ScNiSi_3$,[16] $FeSi_2$,[17] Nd_2Te_5,[18] and the popular PbFCl structure type.

The PbFCl structure is adopted by many, many compounds with bonding ranging from typically ionic to metallic.[19] Nearly 200 phases are known to have the PbFCl structure, and as the synonyms ZrSiS, BiOCl, Cu_2Sb, or Fe_2As show, this type is a true chameleon. We are going to call this structural type generically MAB in this paper, since our primary interest is in compounds where M is a large metal atom and A and B main group elements. We will also refer to this parent structure by the ZrSiS designation.

Table I. MX_2 and MX'X'' Phases Adopting the ZrSiS Structure

Phase	c/a	ref
UNTe	1.939	20
$NdSe_2$	1.997	21
UBi_2	2.004	22
$YbS_{1.7}$	2.016	23
$CeTe_2$	2.018	24
$LaTe_2$	2.025	25
UP_2	2.038	26
UAsSB	2.038	27
USb_2	2.046	28
$PaSb_2$	2.054	29
$ThBi_2$	2.070	30
UPSe	2.072	31
UPS	2.093	31
USbTe	2.097	32
$ThAs_2$	2.099	33
UAsSe	2.103	34
UAsTe	2.103	35
UAsS	2.106	35
$ThSb_2$	2.107	36
AmSbTe	2.124	36
USnTe	2.144	32
NpAsS	2.153	38
$Zr_{3.6}As_{4.3}Se_{2.1}$	2.166	39
UGeS	2.179	32, 40
HfGeTe	2.196	41
HfGeS	2.199	41
USiS	2.199	32, 40
ZrGeS	2.212	41
NbGeSb	2.218	42
$Zr_{3.9}As_{4.2}S_{1.9}$	2.221	39
HfGeSe	2.222	41
ZrGeTe	2.224	41
ZrGeSe	2.232	41
TaSiAs	2.245	43
NbGeAs	2.238	42
NbSiSb	2.248	42
NbSiAs	2.263	42
HfSiS	2.273	41
ZrSiS	2.273	41
HfSiSe	2.292	41
ZrSiTe	2.302	41
HfSiTe	2.651	41

(7) Schubert, K. *Kristallstrukturen zweikomponentiger Phasen*; Springer-Verlag: Berlin, Göttingen, Heidelberg, 1964.
(8) Bärnighausen, H. *Commun. Math. Chem.* **1980**, *9*, 1.
(9) Megaw, H. D. *Crystal Structures: A Working Approach*; Saunders Co.: Philadelphia, 1973; p 282.
(10) Hoffmann, R.; Zheng, C. *J. Phys. Chem.* **1985**, *89*, 4175.
(11) Zheng, C.; Hoffmann, R. *J. Am. Chem. Soc.* **1986**, *108*, 3078.
(12) Trinquier, G.; Hoffmann, R. *J. Phys. Chem.* **1984**, *88*, 6696.
(13) CO on Ni(100): Sung, S.; Hoffmann, R. *J. Am. Chem. Soc.* **1985**, *107*, 578. Methoxy on Cu(100): Zeroka, D.; Hoffmann, R. *Langmuir*, in press. CO/S on Ni(100): Zonnevylle, M.; Hoffmann, R., submitted for publication, *Langmuir*. Oxygen on TiC(100): Jansen, S.; Hoffmann, R., unpublished results.
(14) (a) Grin', Yu. N.; Yarmoluk, Ya. P.; Gladyshevskii, E. I. *Kristallografiya* **1982**, *27*, 686; *Sov. Phys. Crystallogr.* **1982**, *27*, 413. (b) Parthe, E.; Chabot, B. A.; Cenzual, K. *Chimia* **1985**, *39*, 164.
(15) $ScNi_2Si_3$: Kotur, B. Ya.; Bodak, O. I.; Gladyshevskii, E. I. *Kristallografiya* **1978**, *23*, 189; *Sov. Phys. Crystallogr.* **1978**, *23*, 101. UNi_2Si_3: Aksel'rud, L. G.; Lisenko, L. G.; Yarmoluk, Ya. P.; Gladyshevskii, E. I. *Dopov. Akad. Nauk Ukr. RSR* **1977**, *7*, 657.
(16) $ScNiSi_3$: Kotur, B. Ya.; Bodak, O. I.; Mys'kiv, M. G.; Gladyshevskii, E. I. *Kristallografiya* **1977**, *22*, 267; *Sov. Phys. Crystallogr.* **1977**, *22*, 151. $SmNiGe_3$: Bodak, O. I.; Pecharskii, V. K.; Mruz, O. Ya.; Zarodnik, V. Yu.; Vivits'ka, G. M.; Salamakha, P. S. *Dopov. Akad. Nauk. Ukr. RSR, Ser. B* **1985**, (*2*), 36.
(17) Aronsson, B. *Acta. Chem. Scand.* **1960**, *14*, 1414.
(18) (a) Norling, B. K.; Steinfink, H. *Inorg. Chem.* **1966**, *5*, 1488. (b) Pardo, M. P.; Flahaut, J. *Bull. Soc. Chim. Fr.* **1967**, 3658. Pardo, M. P.; Gorochov, O.; Flahaut, J.; Domange, L. *C. R. Hebd. Seances Acad. Sci.* **1965**, *260*, 1666. Lin, W.; Steinfink, H.; Weiss, E. J. *Inorg. Chem.* **1965**, *4*, 877. (c) Chukalin, V. I.; Yarembash, E. I.; Villenskii, A. I. *Izv. Akad. Nauk. SSSR, Neorg. Mater.* **1967**, *3*, 1538; *Inorg. Mater. (Engl. Transl.)* **1966**, *3*, 1341. (d) Bucher, E.; Andres, K.; Maita, J. P.; Cooper, A. S.; Longinotti, L. D. *J. Phys. (Paris) Suppl. C1* **1971**, *32*, 115. (e) Yarembash, E. I.; Vigileva, E. S. *Isz. Akad. Nauk SSR, Neorg. Mater.* **1971**, *7*, 1568; *Inorg. Mater. (Engl. Transl.)* **1971**, *7*, 1388. (f) Yarembash, E. I.; Vigileva, E. S.; Eliseev, A. A.; Zachatskaya, A. V.; Aminov, T. G.; Chernitsyna, M. A. *Izv. Akad. Nauk. SSSR, Neorg. Mater.* **1974**, *10*, 1409; *Inorg. Mater. (Engl. Transl.)* **1974**, *10*, 1212. (g) Cannon, J. F.; Hall, H. T. *Inorg. Chem.* **1970**, *9*, 1639. (h) Damien, D. *Inorg. Nucl. Chem.* **1974**, *36*, 307. (i) Damien, D. *Inorg. Nucl. Chem. Lett.* **1973**, *9*, 453. (j) Damien, D. *Inorg. Nucl. Chem. Lett.* **1972**, *8*, 501. (k) Haase, D. J.; Steinfink, H.; Weiss, E. J. *Inorg. Chem.* **1965**, *4*, 541. (l) Ramsey, T. H.; Steinfink, H.; Weiss, E. J. *Inorg. Chem.* **1965**, *4*, 1154. (m) Lin, W.; Steinfink, H.; Weiss, E. J. *Inorg. Chem.* **1965**, *4*, 877. (n) Damien, D.; Wojakowski, A.; Müller, W. *Inorg. Nucl. Chem. Lett.* **1976**, *12*, 441.
(19) (a) Pearson, W. B. *Z. Kristallogr.* **1985**, *171*, 23. (b) Ptasiewicz-Bak, H.; Leciejewicz, J.; Zygmunt, A. *Phys. Status Solidi* **1978**, *A47*, 347.
(20) Trojko, R.; Despotovic, Z. *Croat. Chim. Acta* **1977**, *47*, 121.
(21) Eliseev, A. A.; Kuznecov, V. G. *Izv. Akad. Nauk SSSR, Neorg. Mater.* **1966**, *2*, 1157; *Inorg. Mater. (Engl. Transl.)* **1966**, *2*, 999.
(22) Leciejewicz, J.; Troc, R.; Murasik, A.; Zygmunt, A. *Phys. Status Solidi* **1967**, *22*, 517.
(23) Teske, C. L. *Z. Naturforsch.* **1974**, *29b*, 297.
(24) (a) Pardo, M. P.; Flahaut, J.; Domange, L. *C. R. Hebd. Seances Acad. Sci.* **1963**, *256*, 953. (b) Pardo, M. P.; Flahaut, J.; Domange, L. *Bull. Soc. Chim. Fr.* **1964**, 3267.
(25) (a) Eliseev, A. A.; Kuznecov, V. G. *Izv. Akad. Nauk SSSR, Neorg. Mater.* **1965**, *1*, 692; *Inorg. Mater. (Engl. Transl.)* **1965**, *1*, 635. (b) Wang, R.; Steinfink, H.; Bradley, W. F. *Inorg. Chem.* **1966**, *5*, 142.
(26) Iandelli, A. *R. C. Accad. Lincei* **1952**, *13*, 138, 144.
(27) Trojko, R.; Despotovic, Z. *J. Nucl. Mater.* **1977**, *67*, 105.
(28) Ferro, R. *R. C. Accad. Lincei* **1952**, *13*, 53.
(29) Hery, Y.; Damien, D.; Charvillat, J. P. *Radiochem. Radioanal. Lett.* **1979**, *37*, 17.
(30) Ferro, R. *Acta Crystallogr.* **1957**, *10*, 476.
(31) Zygmunt, A.; Ligenza, S.; Ptasiewicz, H.; Leciejewicz, J. *Phys. Status Solidi* **1974**, *A25*, K77.
(32) (a) Hulliger, F. *J. Less-Common Met.* **1968**, *16*, 113. (b) Leciejewicz, J.; Zygmunt, A. *Phys. Status Solidi* **1972**, *A13*, 657.
(33) Ferro, R. C. *Acta Crystallogr.* **1955**, *8*, 360.
(34) Pietraszko, D.; Lukaszewicz, K. *Bull. Acad. Pol. Sci. Ser. Sci. Chim.* **1975**, *23*, 337.
(35) Zygmunt, A.; Murasik, A.; Ligenza, S.; Leciejewicz, J. *Phys. Status Solidi* **1974**, *A22*, 75.
(36) Ferro, R. C. *Acta. Crystallogr.* **1956**, *9*, 817.
(37) Charvillat, J. P.; Damien, D.; Wojakowski, A. *Rev. Chim. Miner.* **1977**, *14*, 178.
(38) Wojakowski, A. *J. Less-Common Met.* **1985**, *107*, 155.
(39) (a) Barthelat, J. C.; Jeannin, Y.; Rancurel, J. F. *C. R. Hebd. Seances Acad. Sci.* **1969**, *268*, 1756. (b) Barthelat, J. C.; Jeannin, Y. *J. Less-Common Met.* **1972**, *26*, 273.

In Table I we list some of the known materials having the MAB(ZrSiS) structure. There are several ways to describe this beautiful layering of square nets. Two views are shown in **2** and **3**. There are two associated square nets each of M and B atoms,

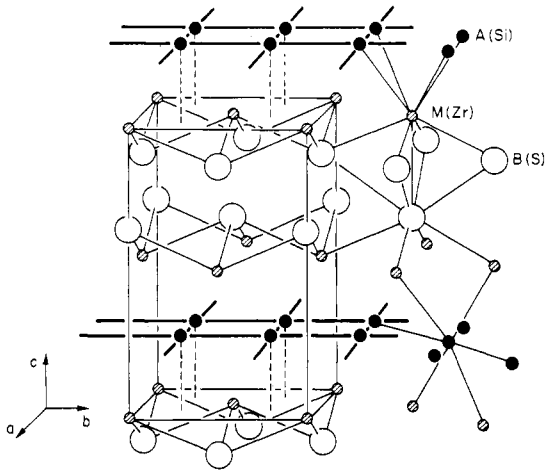

2

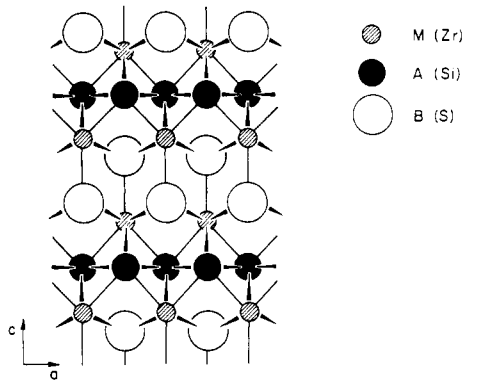

3

separated by a 4^4 layer of A. The A layer is twice as dense as the individual M or B layer, the A–A distance being ≈2.5 Å for A = Si. The metal coordination can be seen in **2**. Four Si and four S atoms form a square antiprism around Zr (Zr–Si = 2.82 Å, Zr–S = 2.65 Å). One square face of this antiprism is capped by another S atom at a distance of 2.83 Å from the Zr.

From another point of view the structure contains double slabs of triangular prisms of A and B atoms parallel to the a,b plane. The prism axes on one slab are along a and along b in the other. Alternate prisms are either centered by M or base centered by A atoms in the common plane joining the double slabs. From still another point of view the structure may be regarded as a distorted cubic close packed array of M atoms with B atoms in the octahedral and A atoms in one-half of the tetrahedral voids. This corresponds to a NaCl structure for $c/a = \sqrt{2}$ and positional parameters of $^3/_4$ and $^1/_4$ for B and M atoms, respectively. The MAB (ZrSiS) structure, however, is severely distorted. If we omit the octahedral cations we obtain an idealized CuTe[44] structure type, and filling the tetrahedral voids leads to the Li_3Bi[45] and ZrCuSiAs[46] structures. One particular feature of the ZrSiS structure is the ability to allow geometrical distortions. These may be stacking variants, as in the UGeTe type,[40,47] or intergrowth of other structural fragments, as in the rare earth tellurides $LnTe_3$[18] or Ln_2Te_5.[18] Among the materials adopting the MAB structure in Table I are found many rare earth compounds LnXY (Ln = rare earth cation; X, Y = anions).

The more ionic compounds in this structural type conform to normal valence rules and are electronically not very interesting. PbFCl itself is a good representative of this extreme, $Pb^{2+}F^-Cl^-$. The more covalent phases are much more interesting. They are often metallic; the contacts between the group 14/15 more dense A layer atoms become bonds of fractional bond order. These bonds will be the focus of our attention.

Several distorted variants of the MAB(PbFCl) structure have been reported. One is the orthorhombic GdPS[48] **4** structure, another one the monoclinic CeAsS[49] structure reported by Hulliger et al. The distortions of the A layers lead to the formation of cis/trans chains with P–P single bonds in GdPS and distorted As–As zigzag chains in CeAsS. These materials are semiconducting Mooser–Pearson phases.[50]

Note that the MAB structure is adopted for different electron counts, e.g., we find representatives ThOS,[51] ThAsS,[32] and $ThAs_2$.[33] Moving to a composition $ThGe_2$[52] we observe a structural change. Here in the so-called $ZrSi_2$ structure type **5**[53,54] the layers are stacked differently, so that half of the non-metal atoms form bonded zigzag chains. In other words, by adding electrons to $ZrSi_2$ we break Si–Si bonds. The $ZrSi_2$ structure can be constructed by inserting infinite trigonal prism slabs of composition ZrSi (as

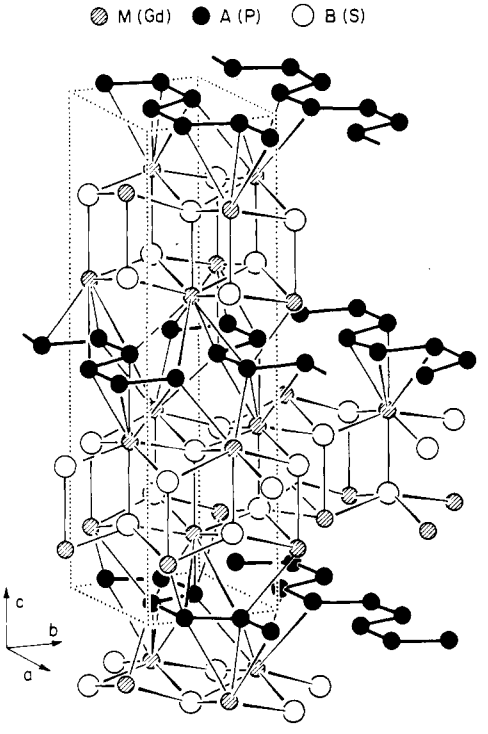

4

(40) Haneveld, A. J. K.; Jellinek, F. *J. Less-Common Met.* **1969**, *18*, 123.
(41) (a) Jellinek, F.; Hahn, H. *Naturwissenschaften* **1962**, *49*, 103. (b) Haneveld, A. J. K.; Jellinek, F. *Recl. Trav. Chim. Pays-Bas* **1964**, *83*, 776. (c) Onken, H.; Vierheilig, K.; Hahn, H. *Z. Anorg. Allg. Chem.* **1964**, *333*, 267.
(42) Johnson, V.; Jeitschko, W. *J. Solid State Chem.* **1973**, *6*, 306.
(43) Hulliger, F. *J. Less-Common Met.* **1973**, *30*, 397.
(44) Karlsson, N. *J. Inst. Met.* **1951**, *79*, 391.
(45) Zintl, E.; Brauer, G. *Z. Elektrochem.* **1935**, *41*, 297.
(46) Johnson, V.; Jeitschko, W. *J. Solid State Chem.* **1974**, *11*, 161.
(47) Stocks, K.; Eulenberger, G.; Hahn, H. *Z. Anorg. Allg. Chem.* **1981**, *472*, 139.
(48) Hulliger, F.; Schmelczer, R.; Schwarzenbach, D. *J. Solid State Chem.* **1977**, *21*, 371.
(49) (a) Sfez, G.; Adophe, C. *Bull. Soc. Fr. Mineral. Kristallogr.* **1972**, *95*, 553. (b) Ceolin, R.; Rodier, N.; Khokadad, P. *J. Less-Common Met.* **1977**, *53*, 137. (c) Schmelczer, R.; Schwarzenbach, D.; Hulliger, F. *Z. Naturforsch.* **1981**, *36b*, 463.
(50) Mooser, E.; Pearson, W. B. *Phys. Rev.* **1956**, *101*, 1608; *J. Electron.* **1956**, *1*, 629; *Prog. Semicond.* **1960**, *5*, 103.
(51) Wyckoff, R. W. G. *Crystal Structures*, 2nd ed.; Wiley-Interscience: New York, 1965; Vol. 1, 2, 3.
(52) Brown, A. *Acta. Crystallogr.* **1962**, *15*, 652.
(53) (a) Schachner, H.; Nowotny, H.; Kudielka, H. *Mh. Chem.* **1954**, *85*, 1140. (b) Vaugh, P. A.; Bracuti, A. *Abstr. Am. Cryst. Assn.*, Summer Meeting, 1955; p 8. (c) Bracuti, A. J. J. *Diss. Abstr.* **1958**, *19*, 1217.
(54) $HfSi_2$, $HfGe_2$, and $ZrGe_2$ crystallize in the $ZrSi_2$ structure as well. See: Smith, J. F.; Bailey, D. M. *Acta. Crystallogr.* **1957**, *10*, 341.

found in the CrB[55] structure type) between square nets of Si atoms. As before for the parent MAB structure we can easily find distorted variants, for instance in the $CaSb_2$ structure type **6**.[56] Here the square net of atoms is broken and the Sb atoms form bonded zigzag chains. Representatives for both structures are $YbSb_2$[57] ($ZrSi_2$ structure type) and $EuSb_2$[58] ($CaSb_2$ structure type). It is suggested that the structure change is triggered by small differences in the valence states for Yb and Eu.

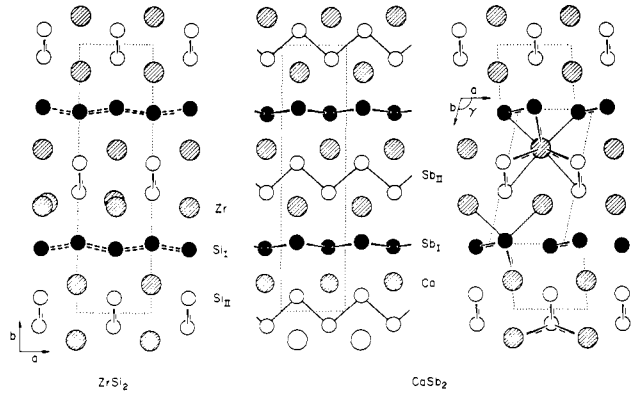

5 **6**

The structural feature we have been following so far, square nets and their distortions, is hardly exhausted by these examples. Consider the ATB_2 structure type exemplified by $SrZnBi_2$, **7**.[59] Using the concept of structural fragment intergrowth[14] we can describe this structure as being built up from $BaAl_4$[60] and α-Po 4^4 layers. The known phases are listed in Table II.

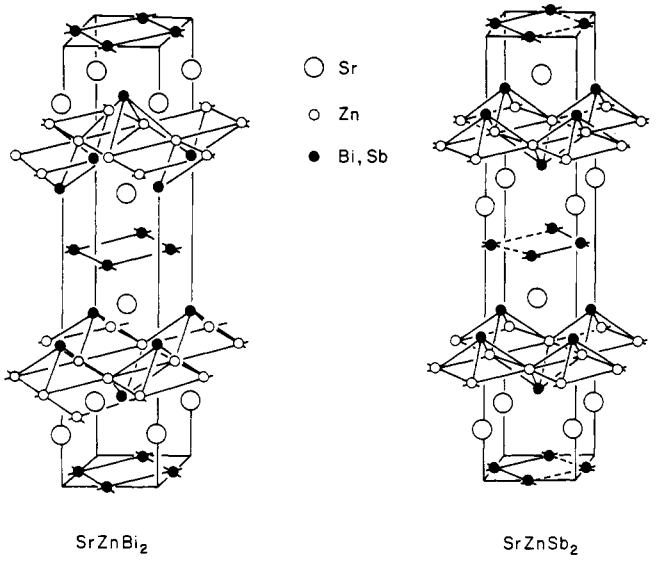

7 **8**

The structure contains layers of edge-sharing TB_4 pyramids. These are separated by layers of A atoms and a square net of B atoms stacked in ABA sequence. Most of these phases do not distort, but in $SrZnSb_2$[64] **8** we find again a distorted variant, where Sb–Sb zigzag chains are formed.

Table II. Materials Adopting the ATB_2 Structure

Phases	c/a	ref
$BaMnSb_2$	5.37	61
$SrMnBi_2$	5.05	61
$BaMnBi_2$	5.23	61
$CaMnBi_2$	2.46	62
$SrZnBi_2$	4.73	59
$SrZnSb_2$		64
$LaZn_{0.52}Sb_2$	2.395	63
$LaCo_{0.68}Sb_2$	2.457	63
$LaMn_{0.76}Sb_2$	2.501	63
$LaCu_{0.82}Sb_2$	2.373	63

Most of these distortions, in the ZrSiS, $ZrSi_2$ and $SrZnBi_2$ structural types, clearly follow a common pattern. The consequence is in most cases a metal to semiconductor transition. The obvious question is the following: why do some of these materials distort and become normal valence compounds, but some do not? What is the underlying electronic driving force?

In a separate contribution[65] we also study the not unrelated GeS → TlI transformation that is important in the chemistry and physics of SnS, SnSe, and related compounds.[66-68]

Building Up the MAB (YbPS) Band Structure

Step by step we build up the electronic structure of the parent lattice. First the square B sublattice is assembled, capped by the metal atoms, and doubled to give a two-dimensional MB lattice. We proceed then to three dimensions by "intercalating" this fragment with some 4^4 A atom nets. Our method of calculation is the extended Hückel method,[69-71] whose parameters are given in the Appendix. A choice of atoms has to be made in this welter of structures. Since one of our main interests was in the distortions exhibited by the LnXS (X = P, As) structures, we chose to carry out the calculations on M = Yb, A = P, B = S, i.e., YbPS in the ZrSiS, GdPS, and CeAsS structures.

The band structure of a two-dimensional lattice of S atoms (S···S = 3.2 Å), which is shown in Figure 1 and schematically in Figure 2, is easily understood. Because of the large S–S separation the bands are relatively flat, to begin with. At the Γ point each orbital has the same sign as its next nearest neighbors' correspondent orbitals. The s band is lowest in energy, next comes the p_z band, and the degenerate $p_{x,y}$ band is pushed up highest because of antibonding nearest-neighbor interaction. At the X point, orbitals in neighboring cells in the x direction and at the M point, orbitals in all nearest neighboring cells change sign. So the s band is expected to go up in energy going from Γ to X to M. The same is true for the p_z band, but its bandwidth has to be smaller because there is π-type overlap instead of σ-type overlap. Moving away from the Γ point the degeneracy of the $p_{x,y}$ band is broken. Changing signs from one unit cell to the next for the p_x band means more σ-bonding interaction, so the p_x band goes down in energy. The p_y band goes up a little bit because of π^* antibonding interaction. Along the line X–M the p_y band is stabilized substantially and p_x now goes up a bit because of antibonding interactions. The p_x and p_y bands meet again at the

(55) Kiessling, R. *Acta Chem. Scand.* **1949**, *3*, 595.
(56) (a) Deller, K.; Eisenmann, B. *Z. Anorg. Allg. Chem.* **1976**, *425*, 104. (b) Deller, K.; Eisenmann, B. *Z. Naturforsch.* **1976**, *31b*, 1146.
(57) (a) Wang, R.; Bodnar, R. E.; Steinfink, H. *Inorg. Chem.* **1966**, *5*, 1468. (b) Bodnar, R. E.; Steinfink, H. *Inorg. Chem.* **1967**, *6*, 327. (c) Bodnar, R. E.; Steinfink, H.; Narasinham, K. S. V. L. *J. Appl. Phys.* **1968**, *39*, 1485.
(58) Hulliger, F.; Schmelczer, R. *J. Solid State Chem.* **1978**, *26*, 389.
(59) Cordier, G.; Eisenmann, B.; Schäfer, H. *Z. Anorg. Allg. Chem.* **1976**, *426*, 205.
(60) (a) Andress, K. R.; Alberti, E. *Z. Metallkd.* **1935**, *27*, 126. (b) Pearson, W. B. *J. Solid State Chem.* **1985**, *56*, 278.
(61) Cordier, G.; Schäfer, H. *Z. Naturforsch.* **1977**, *32b*, 383.
(62) Brechtel, E.; Cordier, G.; Schäfer, H. *Z. Naturforsch.* **1980**, *35b*, 1.
(63) Cordier, G.; Schäfer, H.; Woll, P. *Z. Naturforsch.* **1985**, *40b*, 1097.
(64) Brechtel, G.; Cordier, G.; Schäfer, H. *Z. Naturforsch.* **1979**, *34b*, 251.
(65) Tremel, W.; Hoffmann, R. *Inorg. Chem.*, in press.
(66) Littlewood, P. B., *CRC Crit. Rev. Solid State Mater. Sci.* **1983**, *11*, 229.
(67) Burdett, J. K.; McLarnan, T. *J. Chem. Phys.* **1981**, *75*, 5764.
(68) (a) Wiedemeier, H.; Csielag, F. J. *Z. Kristallogr.* **1979**, *149*, 17. (b) Bucchia, P. S. D.; Jumas, J.-C.; Maurin, M. *Acta. Crystallogr.* **1981**, *B37*, 1903. (c) von Schnering, H.-G.; Wiedemeier, H. *Z. Kristallogr.* **1981**, *156*, 143. (d) Chattopadhyay, T.; Pannetier, J.; von Schnering, H. G. *Z. Kristallogr.* **1985**, *170*, 29.
(69) Hoffmann, R. *J. Chem. Phys.* **1963**, *34*, 1397. Hoffmann, R.; Lipscomb, W. M. *Ibid.* **1962**, *36*, 3179, 3489; **1962**, *37*, 2872.
(70) Ammeter, J. H.; Bürgi, H.-B.; Thibeault, J. C.; Hoffmann, R. *J. Am. Chem. Soc.* **1978**, *100*, 3686.
(71) (a) Whangbo, M.-H.; Hoffmann, R. *J. Am. Chem. Soc.* **1978**, *100*, 6093. (b) Whangbo, M.-H.; Hoffmann, R.; Woodward, R. B. *Proc. R. Soc. London, Ser. A* **1979**, *366*, 23.

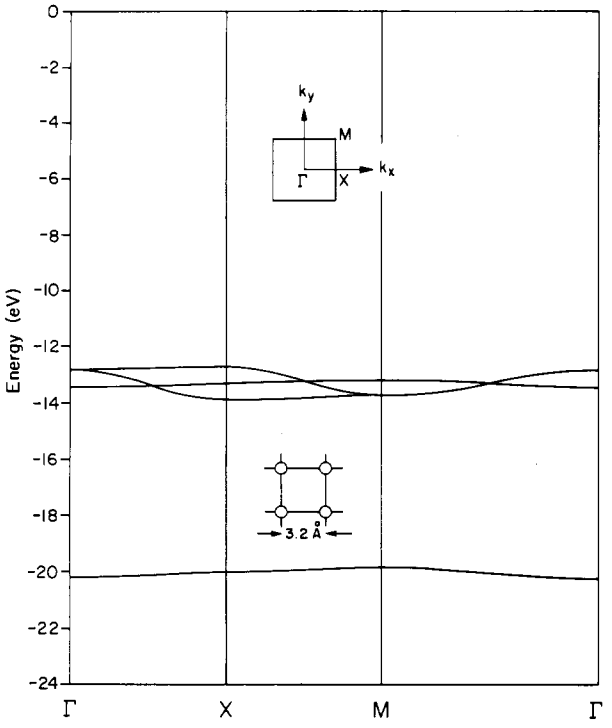

Figure 1. Band structure of a planar square lattice of S atoms. The S···S distance is 3.2 Å. The lattice constant is big enough that s and p bands do not mix.

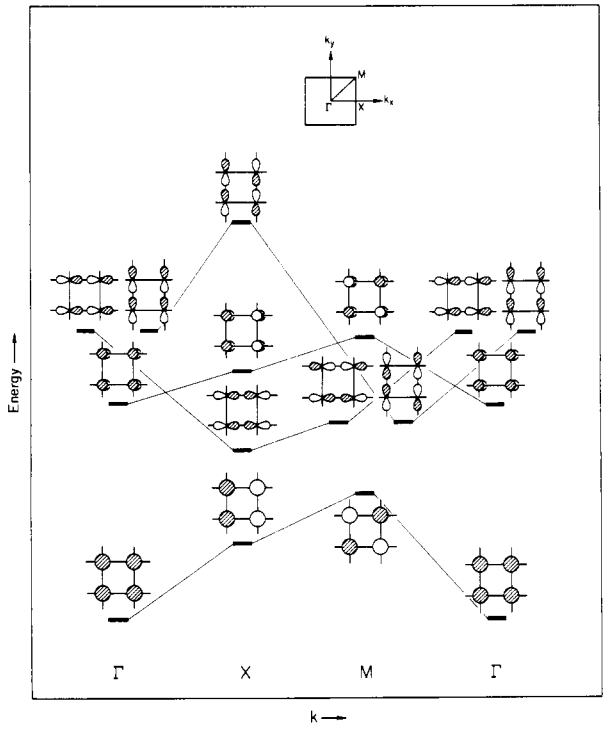

Figure 2. Schematic band structure of a planar square lattice of S atoms. The s and p levels have a large enough separation so that the s and p bands do not overlap.

M point because the symmetry here is D_{4h}, as at the Γ point.

In the next step of our construction we place a metal atom (Yb) on top of the fourfold hollow of the S lattice. The square lattice is still preserved, but as a result of the symmetry reduction (horizontal mirror plane lost) some avoided crossings occur. The resulting band structure is given in Figure 3. The S and Yb centered bands are quite well separated, which we would have anticipated from their very different orbital energies or center of gravities. The general shape of the S bands is unaffected. The small S–Yb interaction that does occur can be rationalized in the

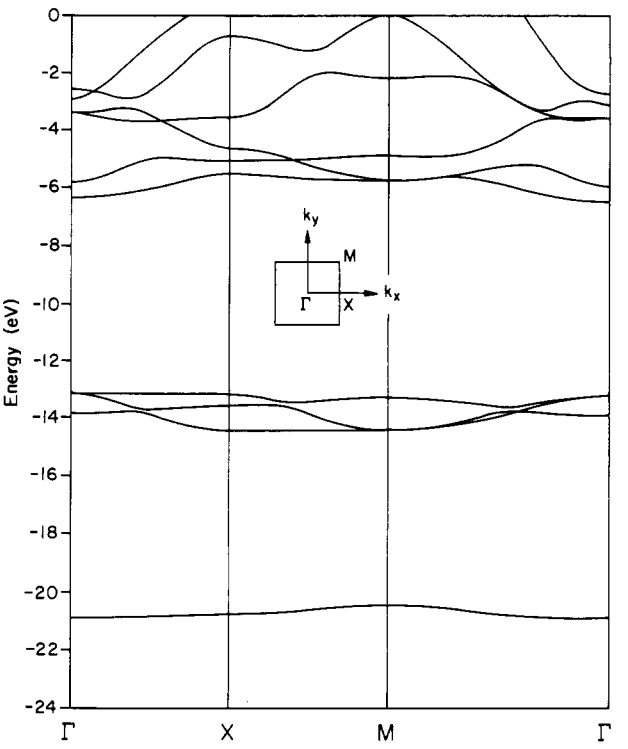

Figure 3. Band structure of a two-dimensional layer of YbS as formed from a planar square lattice of S atoms and apical Yb atoms.

following way: At the Γ point the s and p_z orbitals of the S net have the right topology to interact with the metal s, p_z, and d_{z^2} orbitals, as shown in **9**. The p_x and p_y orbitals of the S net interact with metal p_x and d_{xz} or p_y and d_{yz}, respectively, as indicated for one such interaction in **10**. The strongest interaction is with metal s and p_z orbitals. Since the metal d_{xy} orbitals do not have the

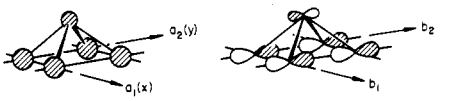

9 **10**

appropriate symmetry to interact with any orbital combination of the square net at the Γ-point, it may be at first surprising to find them pushed up by 2.3 eV in energy compared to the energy of the bare metal orbital. The reason for the destabilization derives from metal–metal interactions, as a band structure calculation on the metal sublattice shows. At the X point the main interaction is between a metal p_x/d_{xz} combination and the s/p_z combination of the square net **11**. The p_x orbitals, of opposite sign to their next nearest neighbors, interact with the metal $s/p_z/d_{z^2}$ combination **12** and the metal d_{xy} orbital has the proper symmetry to interact with the p_y orbitals of the S net **13**. Finally at the M point the main interaction is between metal d_{xy} orbitals and the

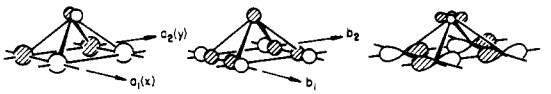

11 **12** **13**

p_z orbitals of the square net **14**, S p_y orbitals interact with the metal p_x/d_{xz} combination **15**, and S p_x orbitals interact with metal p_y/d_{yz} **16**.

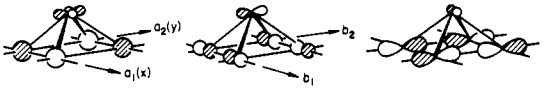

14 **15** **16**

In the next step we put two YbS layers together to construct the YbSSYb slab. In the band structure given in Figure 4 all bands are essentially doubled by forming one symmetric and

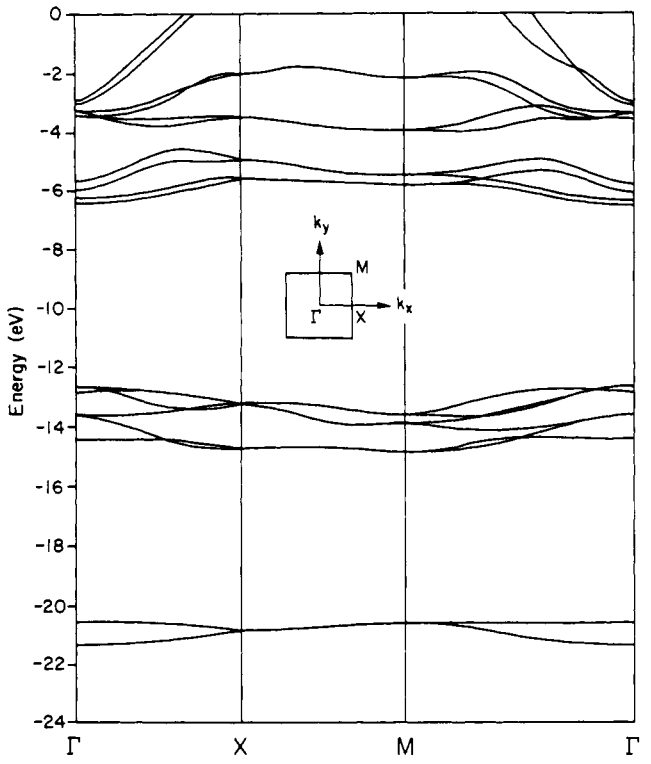

Figure 4. Band structure of a two-dimensional YbSSYb slab is formed by combination of two YbS layers.

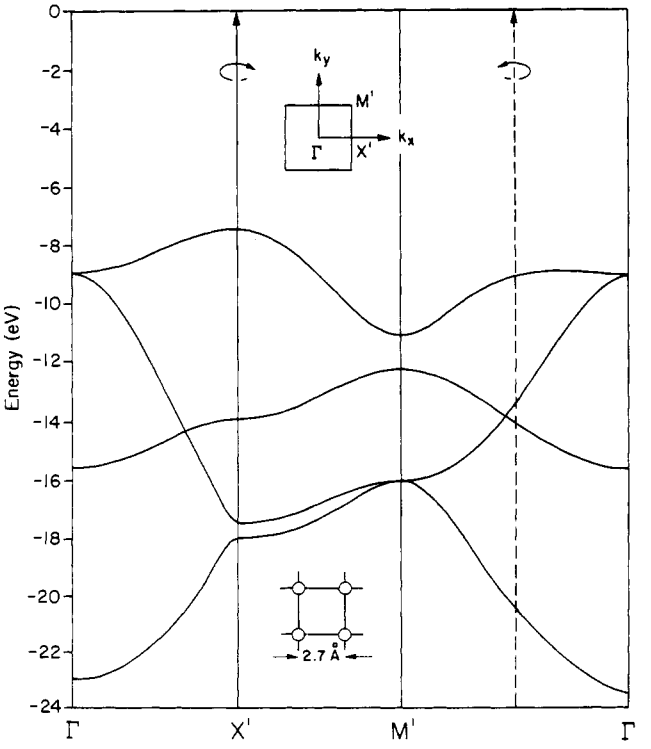

Figure 5. Band structure of a square lattice of P atoms; *k* refers to a glide plane translation. The arrows indicate the rotation axis for the folding back process described in the text.

antisymmetric combination with respect to an n glide plane and all the bands stick together along X–M due to the nonsymmorphic symmetry element.

By using the same modus operandi it is easy to generate the band structure of the 4^4 net of P atoms. The P–P distance of ca. 2.7 Å causes a larger dispersion of the bands, but everything else is the same. The P net in the YbPS unit cell, however, houses two P atoms now instead of one. The second P atom is generated by a face centering, and the band structure of the centered lattice

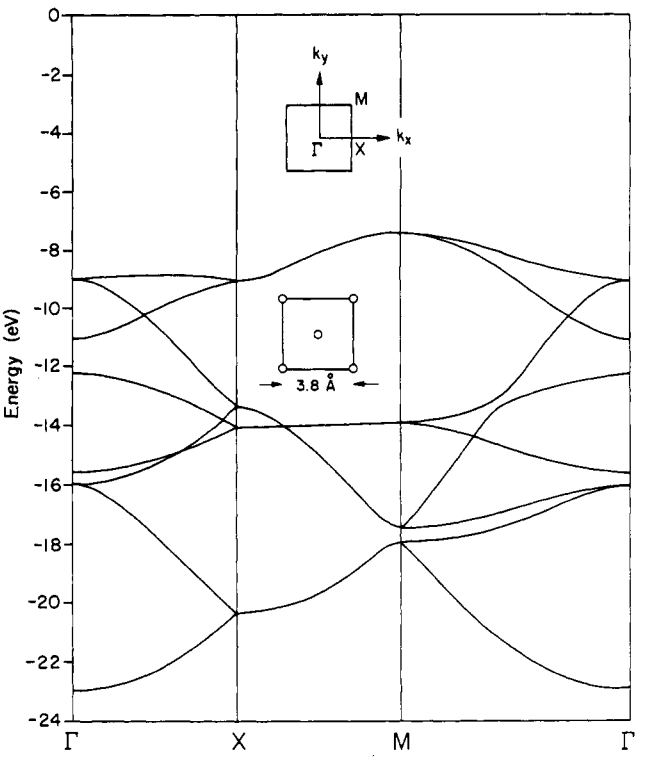

Figure 6. Band structure (after folding back) of a centered square lattice of P atoms as found in the MAB structure.

can be generated from that of the primitive lattice by a simple folding back procedure. The two choices of unit cell—centered and primitive—are given in **17a** and **17b**.

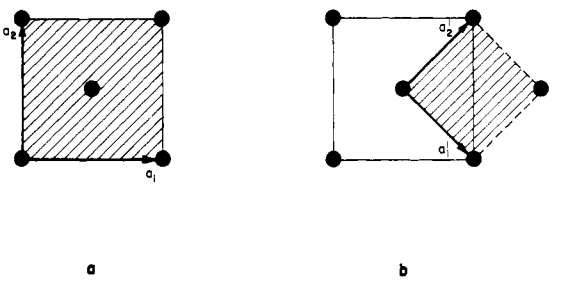

17

The corresponding Brillouin zones (BZs) are shown in **18**, and the band structure of the square lattice shown in Figure 5, **17a**, is plotted along Γ–X′–M′–Γ. The first BZ of the primitive lattice corresponds to the second BZ of the centered lattice. The band structure of the centered cell in Figure 6 can thus be generated by a folding back procedure, which is indicated in Figure 5. If we choose a centered unit cell in the direct lattice as shown in **17a**, the corresponding BZ is the small square X_1', X_2', X_3', X_4' in **18**. Choosing a_1' and a_2' to define the primitive unit cell leaves

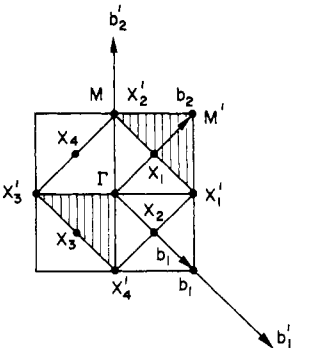

18

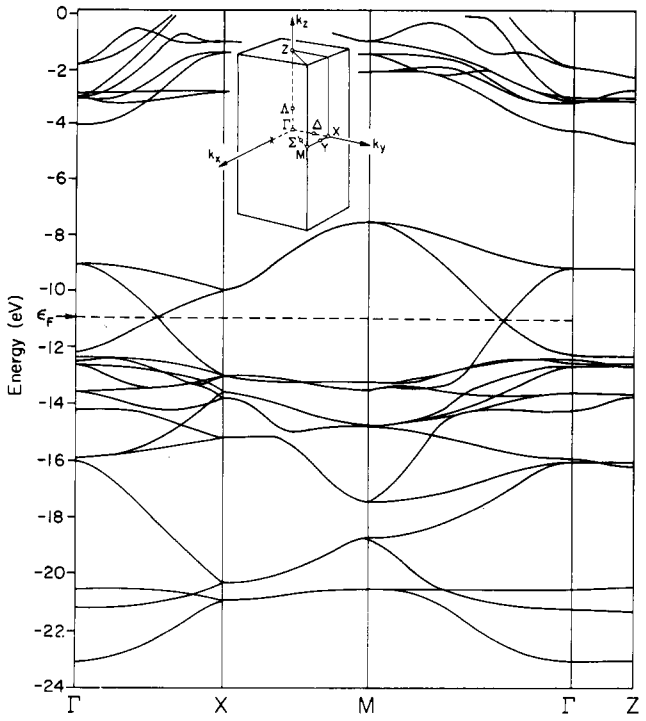

Figure 7. Band structure of YbPS in the MAB (ZrSiS) structure along selected symmetry lines.

us with a BZ twice as large, given by the big square in **18**. The shaded area $X_2'M'X_1'$ in **18** can be translated back to the area $X_3'X_4'\Gamma$, which is equal to $\Gamma X_1'X_2'$ by (time reversal) symmetry. This means that if we map X_1M' on $\Gamma X_1'$ and fold $M'\Gamma$ back so that M' coincides with Γ, we generate the band structure along MΓ and ΓX for the conventional unit cell. The band structure along XM can be sketched by connecting corresponding levels at X and M.

We apologize for the technicalities of the above discussion. Even a simple structure built from square lattices has unavoidable complexities. We give this discussion in detail to assure the reader that it is accessible or understandable in detail and because we need it to study deformations of the lattice, the real chemistry that awaits us.

We proceed to assemble the complete YbPS structure by "intercalating" the YbS and P slabs. The resulting band structure (Figure 7) is interpreted with the help of densities of states (DOS) and their decompositions (Figures 8 and 9) and crystal orbital overlap population (COOP) curves (Figure 10). A word is in order about these. DOS curves are familiar, as are their decompositions into individual atom or orbital contributions. These are alternatively called projections of the DOS or local DOS. The COOP curves are really overlap population weighted DOS curves.[72] They indicate the bonding and antibonding contribution of the levels in a given energy interval, to a specified bond. The integral of the COOP curve up to the Fermi level gives the total overlap population.

The band structure of Figure 7 appears complicated but is in fact easy to analyze. First of all, the electronic structure of YbPS is quite two-dimensional. Whereas there are sizable dispersions along other lines in the BZ, the bands along Γ–Z are flat. The Fermi level crosses two bands in the undistorted YbPS (ZrSiS) structure. These materials should be two-dimensional conductors. This is consistent with the anisotropy in the electrical and magnetic properties of these materials.[73] The band crossing of the Fermi level will, of course, also emerge as the determinant of the distortions these structures undergo.

The band structure of the three-dimensional material bears obvious similarities to that of the slabs that made it up (Figures 4 and 6). The bands at 0 to −4 eV are predominantly Gd d levels. The P and S bands overlay, with attendant avoided crossings, but the general similarity in the shape of the S bands at −21 and −12 to −14 eV in Figures 4 and 7 is apparent. The individual atom contributions to the DOS (Figure 8) confirm this nice separation. The important levels near the Fermi level are in bands clearly derived from the P 4^4 net of Figure 6.

Let us focus on the interactions of the various components of the structure. Yb and S interactions can be followed through the DOS contributions of Figure 8 and the COOP curve of Figure 10. Note the energy regions (−12 to −16, −21 eV) where there is both Yb and S density, and that density is Yb–S bonding. The Yb–P bonding is less obvious, but it may be picked up through the contributions to the DOS of Figure 9. The primary interactions are of P p_z (see the narrow band in the isolated P film broadened) and Yb $d_{xz,yz}$ (note the pushing up in energy of the respective bands).

Of course the strongest interactions are within the dense P layers. Note the wide, highly dispersed P 3s, 3p band (Figure 8), the bottom of which is P–P bonding and the top antibonding (Figure 10). The bands near the Fermi level are strongly P–P antibonding. The conditions for an effective distortion upon symmetry lowering are thus set up. Also it is clear why filling these bands, as in higher electron count structures such as PbFCl, causes rupture of all bonding in the P or B atom layer.

Building up the MAB type phases one has two choices: One is to put S—the more electronegative element—in the more dispersive site in the 4^4 net and P on the fivefold coordinated position. The other choice is to put P in the 4^4 net as in the real structure. The second choice results in a large dispersion in the upper part of the filled bands, because they are localized mainly on P, the less electronegative element. The first choice produces a large dispersion in the lower bands (see **19a**). Having more dispersion in the low-lying filled block creates the solid-state analogue of the 4e repulsive interaction in the molecular case.[11] For the electron count appropriate to YbPS, where some of the P bands are empty, the other choice is much more attractive and in fact we observe for almost all MAB type phases the more electropositive element in the more dispersive site (the 4^4 network). For the PbFCl phases, where all anion bands are filled, this more dispersive site is occupied by the smaller atoms in order to reduce the repulsive interactions. In these materials now the $[Pb_{4/4}F]_n$

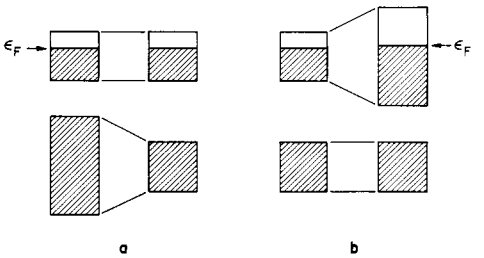

19

sheets are structurally clearly distinguished from the double layers of the bigger anion. The same explanation is valid for the FeOCl phases,[74] a slightly distorted variant of the PbFCl structure. For the metal rich Cu_2Sb or Fe_2As phases these considerations have to be modified.[75]

Distortion of the Square Net

We now focus our attention on the different distorted phases. Let us start with the GdPS structure **5**. As we saw earlier the major deformations that distinguish this structure from the parent

(72) Other applications of COOP curves may be found: (a) Wijeyesekera, S. D.; Hoffmann, R. *Organometallics* **1984**, *3*, 949. (b) Saillard, J.-Y.; Hoffmann, R. *J. Am. Chem. Soc.* **1984**, *106*, 2006. (c) Kertesz, M.; Hoffmann, R. *J. Am. Chem. Soc.* **1984**, *106*, 3453.

(73) Therond, T. G.; Blaise, A.; Fournier, J. M.; Chiapusio, J.; Charvillat, J. P.; Wojakowski, A. *Physica* **1985**, *130B*, 102.

(74) Hulliger, F. In *Structural Chemistry of the Layer-Type Phases*; Levy, F., Ed.; Reidel: Dordrecht, 1976; p 265.

(75) Tremel, W.; Hoffmann, R., unpublished results.

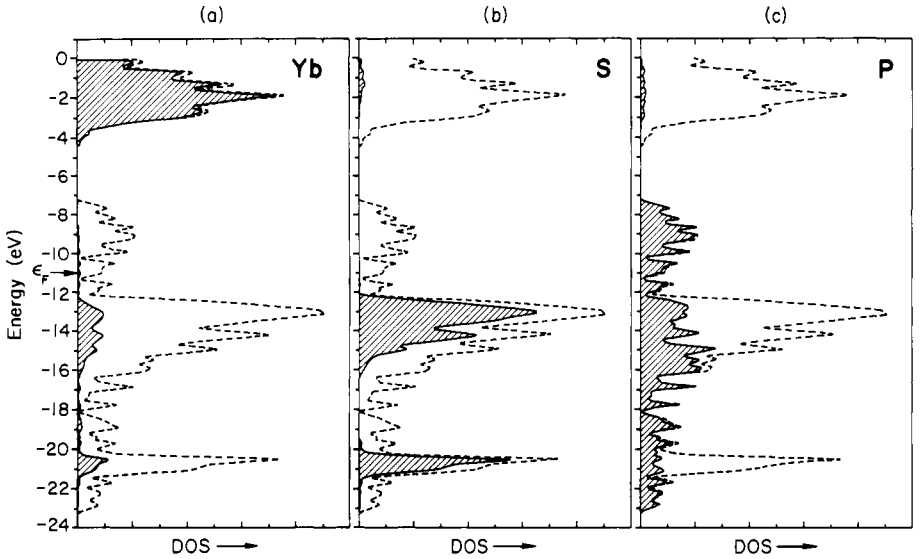

Figure 8. Total DOS (dashed line) and projected DOS (solid line) for YbPS in the MAB (ZrSiS) structure showing (a) metal atom, (b) S atom, and (c) P atom contributions.

MAB or ZrSiS type are motions in the denser A or phosphorus plane forming chains of polyphosphide ions, **20**.

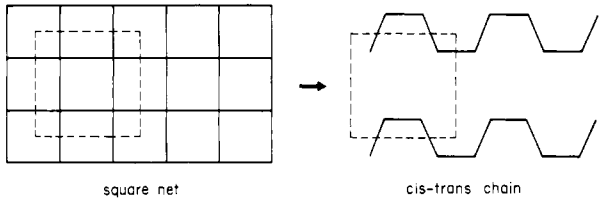

20

In order to discuss the distortion of the parent MAB to the real GdPS structure, we would have to quadruple the unit cell by doubling the square base and the tetragonal axis. Although we do the DOS calculations on the real unit cell, we try in the band structure to keep the unit cell and thus the number of bands as small as possible. Considering the layer-like character of the material, it matters little if we choose a model unit cell with no doubling of the tetragonal axis instead of the real structure **5**. For the symmetry classification of the bands we do have to take into account the different space group (monoclinic $P2_1/m$ instead of *Pmnb*). This means that in order to prepare for the distortion the unit cell has to be doubled. The modus operandi is very similar to that utilized in our previous discussion of the P square lattice. The small and big unit cell are given in **17**, and the corresponding BZs are the same as in **18**. The backfolding process is exactly the same as before. Mapping back M′X′ on X′Γ and folding back ΓM′ onto itself in such a way that M′ coincides with Γ generates the band structure of the big MAB unit cell along the symmetry lines MΓ and ΓX. The resulting band structure is shown in Figure 11a.

The preparation for the distortion has not yet opened up a bandgap at the Fermi level. But the symmetry reduction from tetragonal to monoclinic on going from the MAB to the GdPS structure already implies; however, such a band gap will open up. The driving force for the distortion is revealed by examining the symmetry properties of the space groups of both the undistorted and distorted phase. For our present purpose it may be sufficient to determine which symmetry element is lost in the distortion. A more formal way is to use the maximal group–subgroup relationships.[76] Just from looking at the P slab fragment during the

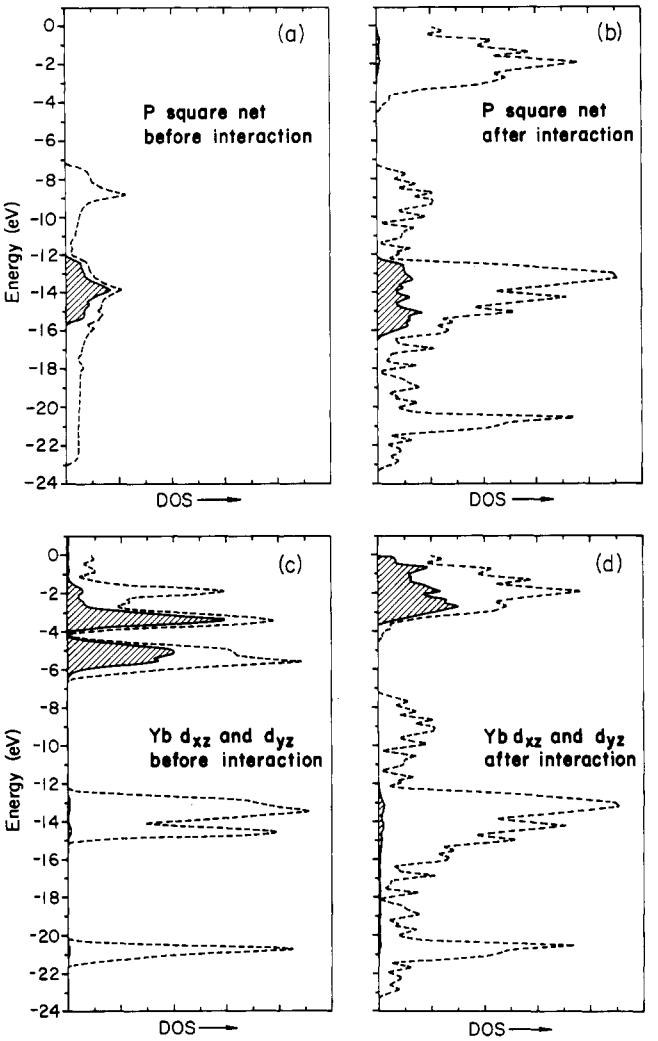

Figure 9. Total density of states (DOS, dashed line) and projected DOS (solid line) illustrating the "intercalation" of a YbSSYb slab between layers of P atoms to form the MAB (YbPS) structure. Top row: projection of the P p_z orbitals (normal to the square net of P atoms) (a) before and (b) after interaction. Bottom row: projections of d_{xz} and d_{yz} orbitals of Yb atoms in the YbSSYb slab (c) before and (d) after interaction.

distortion, it is apparent that the group of k along ΓX in the undistorted structure is C_{2v}, in the distorted structure just C_2. In

(76) (a) Neubüser, J.; Wondratschek, H. *Krist. Tech.* **1966**, *1*, 529. (b) *International Tables for Crystallography*; Hahn, T., Ed.; D. Reidel: Dordrecht (Holland), Boston (USA), 1983; Vol. A. (c) Burzlaff, H.; Zimmermann, H. *Kristallographie: Grundlagen und Anwendungen*, Thieme Verlag: Stuttgart, 1977; Bd. 1.

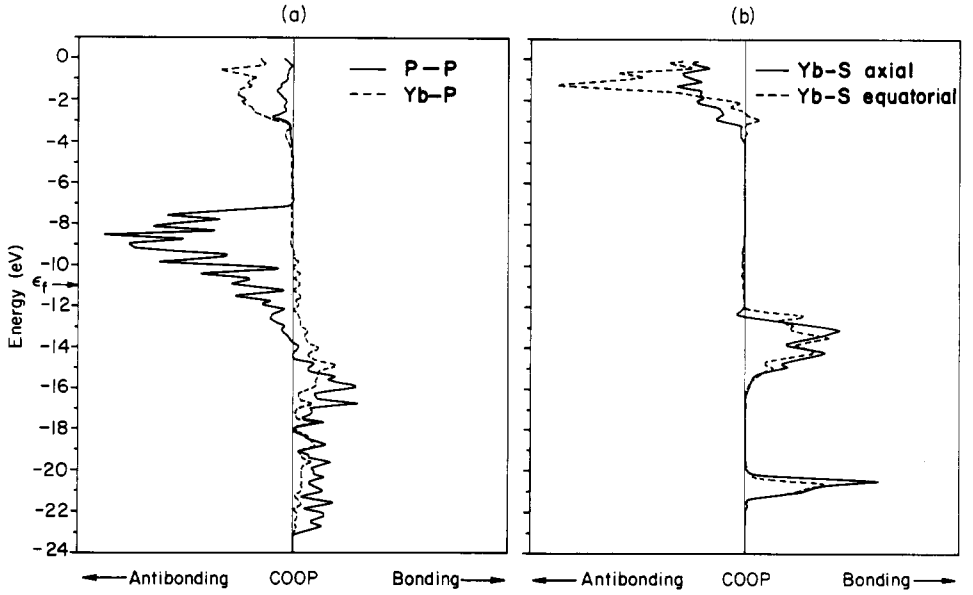

Figure 10. Crystal orbitals overlap population (COOP) curves for the MAB structure (YbPS): (a) (—) P–P bond, (---) Yb–P bond; (b) (—) Yb–S bond (axial), (---) Yb–S bond (equatorial).

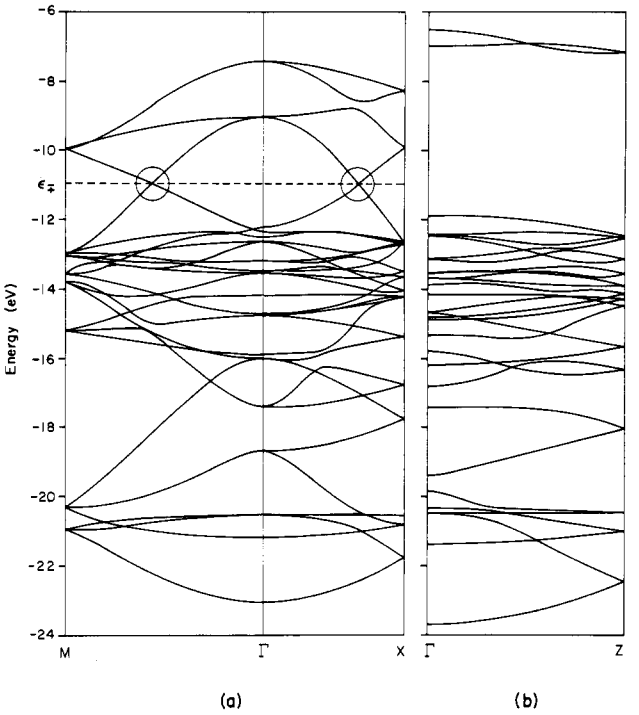

Figure 11. (a) Band structure of YbPS in the ZrSiS structure (after folding back) in a nonprimitive unit cell along M–Γ–X. The nonprimitive structure is "prepared for distortion" to the GdPS structure. (b) Band structure of YbPS in the GdPS structure along the line Γ–Z (corresponds to Γ–X of the nonprimitive ZrSiS unit cell in part a). As a consequence of the symmetry reduction in the MAB(ZrSiS) → GdPS structure distortion a band gap has opened up.

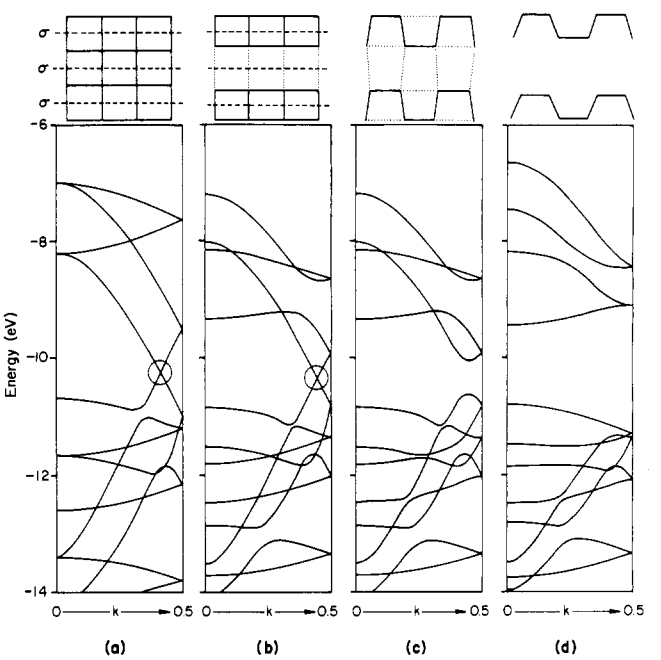

Figure 12. Evolution of the band structure of a square planar model lattice of P atoms, when the MAB(ZrSiS) → GdPS distortion is carried out in three steps. The essential symmetry element (mirror plane) is indicated, and the crucial band crossing is circled. (a) Band structure of an ideal square lattice with full tetragonal symmetry. (b) After symmetry reduction to an orthorhombic system. The mirror plane is still preserved and the band crossing is still present. (c) After beginning distortion to a cis–trans chain. The mirror plane is gone and an avoided crossing occurs at the Fermi level. (d) After the distortion is complete.

other words, in the distortion a mirror plane parallel to the *b* axis is lost. The only symmetry element which is preserved is a 2_1 screw axis (or a glide plane). Therefore we expect bands that were symmetric or antisymmetric with respect to the mirror plane in the high-symmetry structure to mix in the distorted structure.

The result is obvious in the real, distorted GdPS band structure along the line ΓX in Figure 11b. The band crossing has disappeared, and a gap has opened up. The distortion can be thought of proceeding in two steps. In the first step the tetragonal symmetry is lost. The lattice symmetry is orthorhombic, and the crucial mirror plane is still present. In the second step this mirror plane is removed, resulting in a symmetry reduction from orthorhombic to monoclinic. This is consistent with a pathway

$$P4/nmm \xrightarrow{t2} Pmmn \xrightarrow{t2} P2_1/m$$

given by the maximal group–subgroup relationship.[76]

We showed earlier that the important levels near the Fermi level are localized in the square P net. Therefore let us see if the essential features of the distortion can be modelled with a square net of P atoms. The band structure for that square net is given in Figure 12a; then in Figure 12b the symmetry is reduced to orthorhombic but the crucial band crossing is still present. Moving on now to a monoclinic system, a mirror plane is removed, the

bands start mixing, and a band gap opens up (Figure 12c), which develops further, as the distortion proceeds (Figure 12d). Each band is represented at X by a degenerate set of crystal orbitals. The essential crystal orbitals for the undistorted cell are drawn out in **21** and **22**. The combination 11/12 in **21** is symmetric and

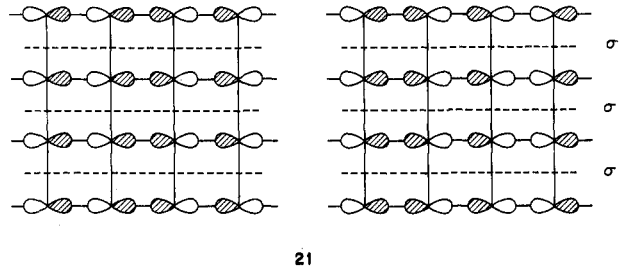

21

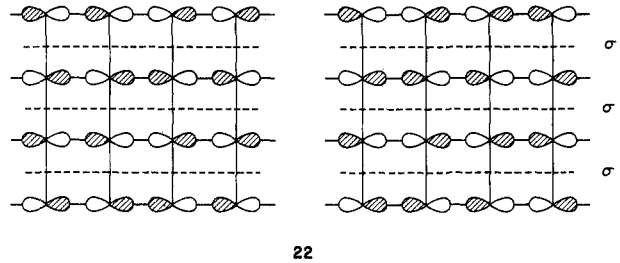

22

13/14 in **22** antisymmetric with respect to the mirror plane *m*. Therefore the bands are allowed to cross in the undistorted structure. In the distorted structure, however, the bands mix. The resulting crystal orbitals are shown in **23** and **24**. One combi-

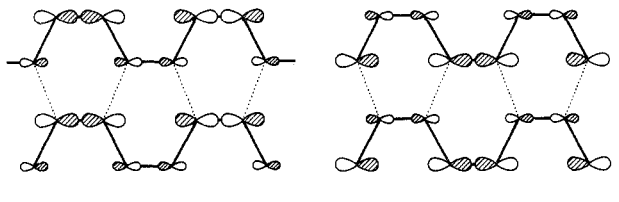

23

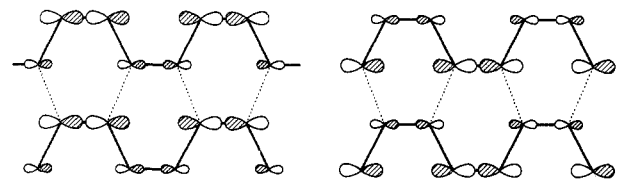

24

nation, **23**, reinforces bonding interactions and drops in energy, the other combination, **24**, is destabilized and pushed up. The result is a rupture of the square P net and the formation of P–P single bonds in a cis–trans polyphosphide chain. The corresponding pattern in the band structure can be seen in Figure 12.

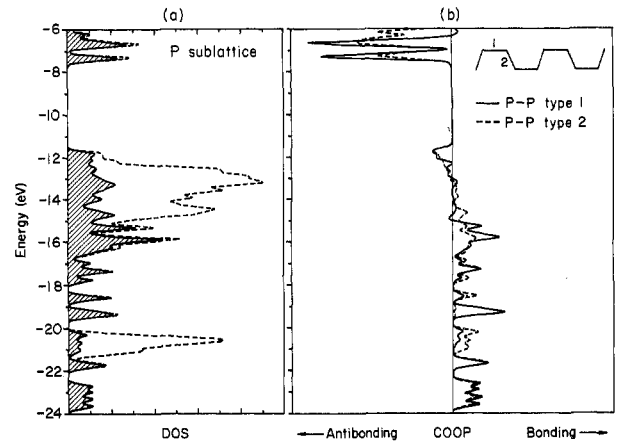

Figure 13. Total DOS (dashed line) and projected DOS (solid line) for YbPS in the GdPS structure showing (a) P atom contribution (b) COOP curves for the P–P bonds.

The situation is clear now and we confirm this picture by looking at the P–P COOP curve and the P contribution of the total DOS in the GdPS structure in Figure 13. A bandgap of ca. 2 eV is produced and some P states are pushed up above the Fermi level. The COOP curve in Figure 13b reveals the P–P antibonding character of these states.

The GdPS structure is not the only possible deformation of the parent MAB structure. Three possible distortions as suggested by Hulliger et al.[48] are sketched in **25**. One is a hypothetical four-ring formation in the P net, the second the GdPS, and the third the CeAsS structure we now proceed to discuss.

In the CeAsS structure, as in GdPS, the unit cell is doubled, here in the *c* direction. The real cell has only monoclinic symmetry. The reason is that the P zigzag chain which results from a simple distortion of the tetragonal lattice is slightly distorted further. Going from a square lattice of atoms as in MAB (space group: $P4/nmm$) to a zigzag chain, the tetragonal symmetry is lifted. In addition, a mirror plane present in the *ac* plane of the MAB structure is removed. This takes us by a t2 step to the space group *Pmmn* in the distorted structure. In this group, however, the *z*(P) parameter is no longer fixed and a doubling of the *c* axis is required. This is essentially what we find in the CeAsS phases. One further step of symmetry reduction then leaves us in the monoclinic system for the real CeAsS phases.

Following this line of thought, we can already tell that the loss of the mirror plane causes mixing of just those bands which cross at the Fermi level in the high-symmetry structure. An orbital explanation (using again the square lattice of P atoms) is easily given. Again at X each orbital is represented by a degenerate set of crystal orbitals (note that this X is different from the X in the GdPS structure before, since unit cells and BZs are different). These are shown for the degenerate pairs 11/12 and 15/16 in **26** and **27**. In the MAB structure both have different symmetry with respect to the mirror plane. As soon as the overall symmetry is reduced, both bands mix. One combination **28** drops

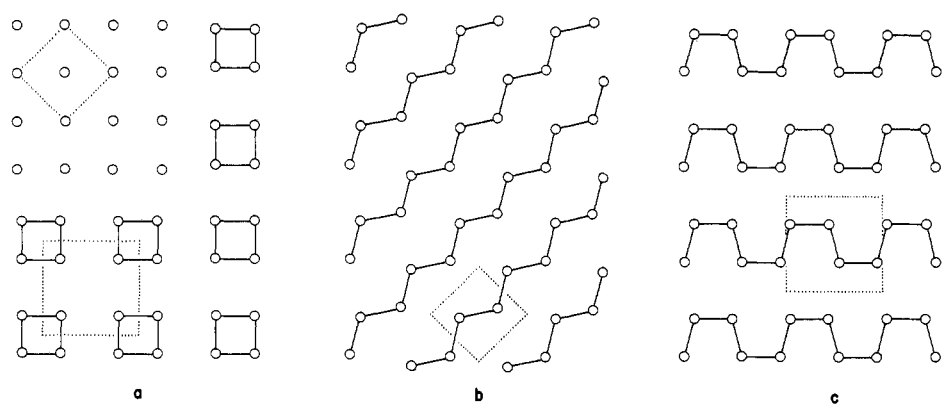

25

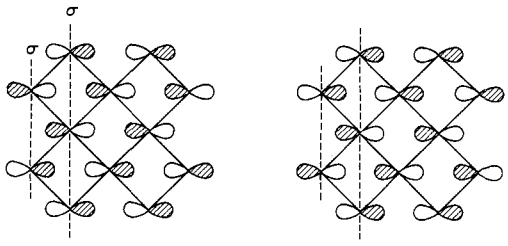

26

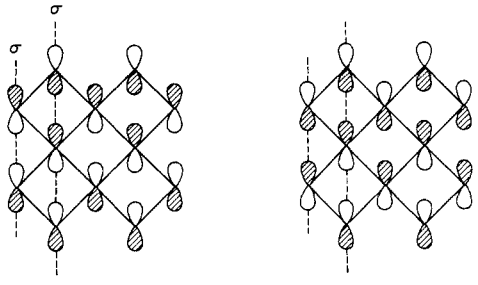

27

in energy and the other one **29** moves up.

What we have given here is a rationale for the distortion by an orbital symmetry picture for one particular *k*-point in the BZ. Next we have to show that our conclusions are valid at any point in the BZ. We have shown the band crossing at the Fermi level to disappear along the line ΓX. Since ΓM is not a symmetry line in any symmetry lower than tetragonal, the crossing along ΓM must be gone as well. Avoided crossings along lines of high symmetry makes band crossings at other points in the BZ impossible. We have also averaged over the BZ and looked at the DOS diagrams and COOP curves for the idealized CeAsS structure. The overall picture is very similar to the GdPS case, and we do not show those diagrams here. As for the GdPS structure, the formation of P chains opens a gap at the Fermi level: some bonding states are pulled below the Fermi level, some antibonding states are pushed up.

There are other distortions of the parent MAB structure. We have already mentioned the tetramer formation **25a**. Although P_4 units are well-known from the skutterudite structures,[77] no MAB structure incorporating their deformation appears to be known. Qualitatively, there seems to be nothing wrong with this type of distortion. Another high-symmetry variant of a distortion is found on the NdAsSe structure.[49c]

Many Related Structures, Some Distorted, Some Not

After providing an orbital picture for two observed distortions of the MAB structure, we will have to answer the question why some phases distort and some do not. In trying to provide an answer for the rare earth (RE) compounds we run into a difficulty. We can certainly include 4f orbitals in our calculations (we did actually in some cases). But we do not always get their position in energy right. Furthermore, our one-electron method cannot handle the complexity of RE spin states and magnetism. What we have to do is to assume a certain filling of the 4f bands and a specific electronic state for the RE atom from the reported physical data or chemical knowledge of the oxidation states encountered in various RE materials and do the calculation using these assumptions. Since the narrow 4f bands do not interact very much with the orbitals of the metalloid, we can ignore them in the following discussion.

Our basic picture is simple for GdPS. Assuming an oxidation

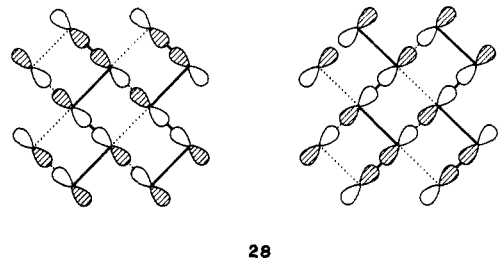

28

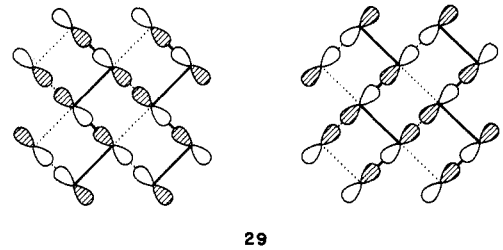

29

state of 3^+ for the Gd atoms (f^7 configuration), all bands up to #14 in Figure 7 are filled in the parent MAB structure. As the lattice distorts, bands #14 and #15 mix and a band gap opens up at the Fermi level. In other words, if we reach a critical electron count, the lattice is stabilized by the distortion. Taking one electron out of the valence band stabilizes the undistorted compound. Materials of composition LnP_2 or LnSiS are not reported to our knowledge. The reduced case, however, is known and RES_2 compounds are found in complicated superstructures of the ZrSiS cell.[78]

Replacing phosphorus and sulfur by higher group homologues should have as a consequence a diminution of the gap between metal 5d states and the valence band. If the valence band overlaps the metal bands, additional electrons do not enter the antibonding part of the valence band and metal bands are filled instead. Therefore the undistorted structure should be preferred in this case. For the lanthanide series the gap between metal 5d and valence band is always too large and we cannot give any relevant example. But compounds of the ZrXY, HfXY (X = Si, Ge; Y = S, Se, Te) series[41] and NbXY (X = Si, Ge; Y = As, Sb)[42] and TaSiAs[43] prefer without exception the undistorted structure. A comparison of the coulomb integrals of Zr and Si atoms shows that this is a consequence of the overlap of valence band and the metal d block.

Pulling the upper part of the valence band down in energy by substituting As or P for Si and adding one more electron, we encounter some complicated borderline cases. $VP_{1.75}$ and $NbP_{1.7}$, a high pressure defect variant of the MAB structure, still prefer the high-symmetry structure,[79] whereas in the $NbAs_2$ type the lattice is completely different.[80] Adding still more electrons to compounds in the MAB (ZrSiS) structure, either metal states or antibonding states of the square net can be occupied. In the first case the structure might remain unchanged; in the latter case we expect a distortion of the square net resulting from the breaking of P–P bonds. This seems to be the case in the NbPS structure

(77) For skutterudite structures MP_3 see: (a) Kjekshus, A.; Rakke, T. *Acta Chem. Scand.* **1974**, *A28*, 99. (b) Rundqvist, S.; Ersson, N. O. *Ark. Kemi* **1968**, *30*, 103. (c) Zuravlev, N. N.; Zhdanov, G. S. *Sov. Phys. Crystallogr.* **1956**, *1*, 404. For the filled scutterudite version LnT_4P_{12} see: (d) Jeitschko, W.; Braun, D. J. *Acta Crystallogr.* **1977**, *B33*, 3401. (e) Braun, D. J.; Jeitschko, W. *J. Solid State Chem.* **1980**, *32*, 357. (f) Braun, D. J.; Jeitschko, W. *J. Less-Common Met.* **1980**, *72*, 147.

(78) Dugue, P. J.; Carre, D.; Guittard, M. *Acta. Crystallogr.* **1978**, *B34*, 403.

(79) Jeitschko, W.; Donohue, P. C.; Johnson, V. *Acta Crystallogr.* **1976**, *B32*, 1499.

(80) Furuseth, S.; Kjekshus, A. *Acta Crystallogr.* **1965**, *18*, 320. For other compounds in the $NbAs_2(OsGe_2)$ structure see: Hulliger, F. *Nature (London)* **1966**, *204*, 775 (MP_2: M = V, Nb, Ta, W; MAs_2: M = V, Mo, W). Rundqvist, S. *Nature (London)* **1966**, *204*, 847 (MP_2: M = Nb, Ta, W). Meissner, H.-G.; Schubert, K. *Z. Metallkd.* **1965**, *56*, 523 (VAs_2). Sanii, G. S.; Calvert, L. D.; Taylor, J. B. *Can. J. Chem.* **1964**, *42*, 63 ($NbAs_2$, $TaAs_2$). Furuseth, S.; Kjekshus, A. *Acta Crystallogr.* **1965**, *18*, 1180 ($NbAs_2$, $TaAs_2$). Furuseth, S.; Kjekshus, A. *Acta Crystallogr.* **1965**, *19*, 95, ($TaAs_2$, $TaSb_2$). Furuseth, S.; Kjekshus, A. *Nature (London)* **1964**, *203*, 512 ($NbAs_2$, $NbSb_2$). Jeitschko, W.; Donohue, P. C. *Acta. Crystallogr.* **1973**, *B29*, 783 (CrP_2, $CrAs_2$). Brown, A. *Nature (London)* **1965**, *206*, 502 ($MoAs_2$). Taylor, J. B.; Calvert, L. D.; Hunt, M. R. *Can. J. Chem.* **1965**, *43*, 3045 ($MoAs_2$, WAs_2). Jensen, P.; Kjekshus, A.; Skansen, T. *Acta Chem. Scand.* **1966**, *20*, 403 ($MoAs_2$, WAs_2). Weitz, G.; Born, L.; Hellner, E. *Z. Metallk.* **1960**, *51*, 228 ($OsGe_2$).

30[81] where two electrons have been added to the parent MAB (ZrSiS) lattice. Note that the NbS slab here is slightly different from the ZrS slab in the parent structure. The bicapped trigonal prismatic metal coordination, however, is still preserved. The stacking pattern corresponds to that in the UGeTe structure (compare the space groups $I4/mmm \leftrightarrow Immm$). In the NbPS structure **30** we observe a distorted 4^4 net of P atoms with long P–P distances of 3.44 Å along the *c* direction and chains with alternating short (2.21 Å) and intermediate (2.57 Å) distances along *b*. This pattern appears to be halfway between a S_n and a Cl_2 analogue. A corresponding electron count may be $Nb^{3.5+}P^{1.5-}S^{2-}$. This implies that some electrons enter the metal d block. Band structure calculations which are the subject of a separate contribution[82] show this simple picture to be qualitatively correct. The isoelectronic material WP_2,[80] however, crystallizes in the $NbAs_2$ structure. We conclude that the preference for one of these structure types depends on a fine balance of electronegativity and size factors.

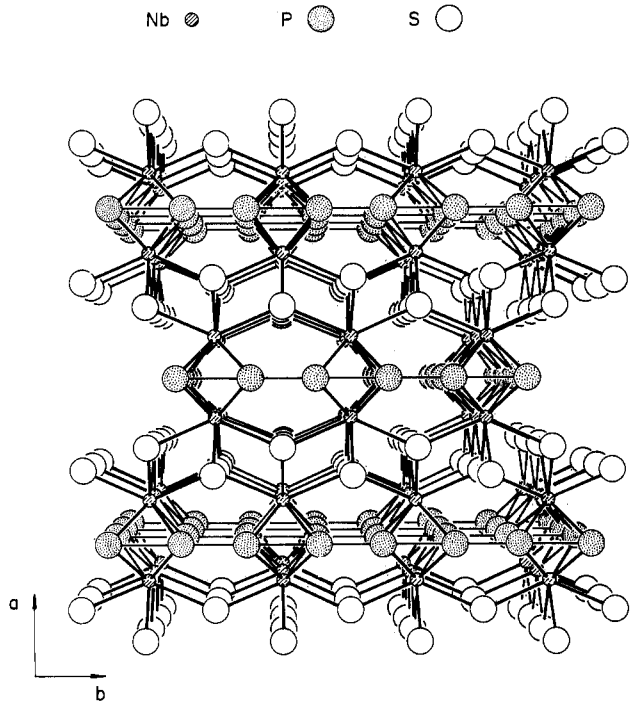

NbPS

30

At this point it might be interesting to note the close resemblance of the $NdTe_3$ **31**[18] or the well-known $ZrSe_3$ structure type **32**[83] with the ZrSiS type. In both structure types basically an additional 4^4 net or non-metal atoms has been inserted. Whereas the square nets are undistorted in the $NdTe_3$ case, they distort in the $ZrSe_3$ structure and the reason is obvious again. In the latter structure metal and non-metal bands are nicely separated; as a consequence of the distortion the valence band is just filled and the material is semiconducting.

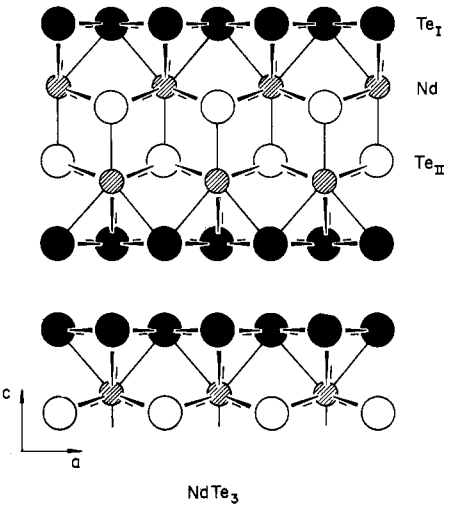

$NdTe_3$

31

Moving on to $NbSe_3$, **33**, or $TaSe_3$,[85] the structure distorts further; the next electron occupies the metal d block, and the large dispersion of the lowest metal band[86] makes this material a good one-dimensional conductor.[87] From **32** the crucial symmetry element that is lost on distortion can easily be determined. It is a mirror plane perpendicular to the *a* axis.

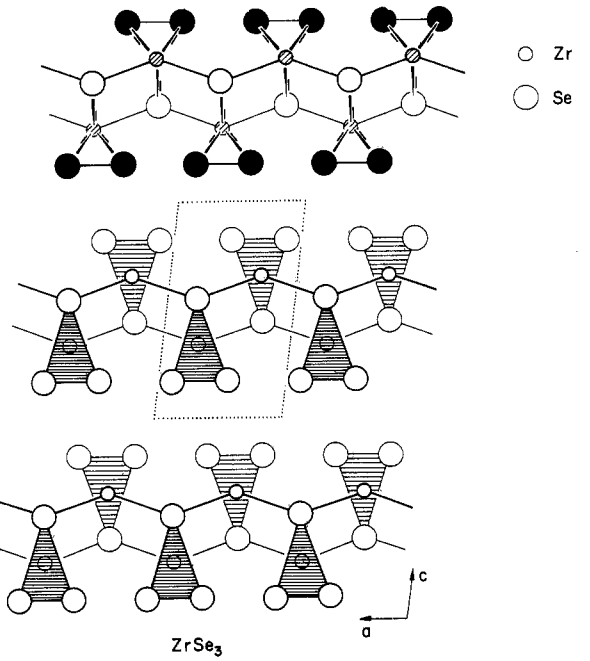

$ZrSe_3$

32

A very interesting point is that a second varient of the $ZrSe_3$ structure exists.[88] Both types A and B differ only in the *x*

(81) Donohue, P. C.; Bierstedt, P. E. *Inorg. Chem.* **1969**, *8*, 2690.
(82) Keszler, D. A.; Hoffmann. R. *J. Am. Chem. Soc.*, preceding paper in this issue.
(83) $ZrSe_3$: Krönert, W.; Plieth, K. *Z. Anorg. Allg. Chem.* **1965**, *336*, 207. MX_3 (M = Ti, Zr, Hf; X = S, Se, Te): Haraldsen, H.; Kjekshus, A.; Rost, E.; Steffensen, A. *Acta Chem. Scand.* **1963**, *17*, 1283. Grimmeis, H. G.; Rabenau, A.; Hahn, H.; Ness, P. *Z. Elektrochem.* **1965**, *65*, 776. Brattas, L.; Kjekshus, A. *Acta Chem. Scand.* **1972**, *26*, 3441. $ThTe_3$: Graham, J.; McTaggart, F. K. *Aust. J. Chem.* **1960**, *13*, 67. US_3: Suski, W.; Trzebiatowski, W. *Bull. Acad. Pol. Sci., Ser. Sci. Chim.* **1964**, *12*, 277. Picon, M.; Flahaut, J. *Bull. Soc. Chim. Fr.* **1958**, 778. Grønvold, F.; Haraldsen, H.; Thurmann-Moe, T.; Tufte, T. *J. Inorg. Nucl. Chem.* **1968**, *30*, 2117. USe_3: Khodadad, P. *Bull. Soc. Chim. Fr.* **1961**, 133. Ellert, G. V.; Slovyanskikh, V. K. *Z. Neorg. Khim.* **1974**, *19*, 1389; *Russ. J. Inorg. Chem.* **1974**, *19*, 756. Slovyanskikh, V. K.; Yarembash, E. I.; Ellert, G. V.; Eliseev, A. A. *Itv. Akad. Nauk. SSR, Neorg. Mater.* **1968**, *4*, 624; *Inorg. Mater. Isv. (Engl. Transl.)* *4*, 543. NpS_3: Marcon, J. P. *C. R. Hebd. Seances Acad. Sci.* **1967**, *265C*, 235. $NpSe_3$: Damien, D.; Damien, N.; Jove, J.; Charvillat, J. P. *Inorg. Nucl. Chem. Lett.* **1973**, *9*, 649.
(84) Meerschaut, A.; Rouxel, J. *J. Less-Common Met.* **1975**, *39*, 197. Hodeau, J. L.; Marezio, M.; Roucea, C.; Ayroles, R.; Meerschaut, J.; Rouxel, J.; Monceau, P. *J. Phys. C: Solid State Phys.* **1978**, *11*, 4117.
(85) Bjerkelund, A.; Fermov, J. H.; Kjekshus, A. *Acta Chem. Scand.* **1966**, *20*, 1838.
(86) (a) Bullett, D. W. *J. Phys. C: Solid State Phys.* **1977**, *12*, 277; *Solid State Commun.* **1978**. *26*, 563. (b) Hoffmann, R.; Shaik, S.; Scott, J. C.; Whangbo, M.-H.; Foshee, M. *J. Solid State Chem.* **1980**, *34*, 263.
(87) For a recent review see: Grüner, R. *Comments Solid State Phys.* **1983**, *10*, 183.
(88) Furuseth, S.; Brattas, L.; Kjekshus, A. *Acta Chem. Scand.* **1975**, *A29*, 623.

parameter ($x_A = -x_B$), so that variant B corresponds to a kind of mirror image (symmetry plane parallel to (100) at $x = {}^1/_2$).

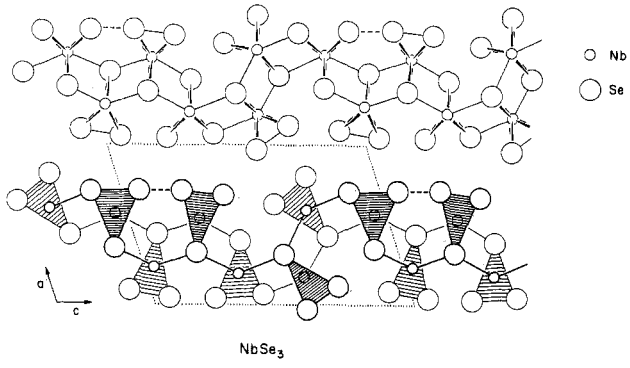

33

The deviation of the monoclinic angle β from 90° prevents a perfect left/right identity between the two variants. Kinetic factors related to crystal growth from the vapor phase were believed to be responsible for the two variants. To our knowledge twinned structures have not been described. The existence of these "enantiomers" suggests that one might be able to obtain the undistorted material as a high-temperature phase.

For the LnAsS series, metal 5d block and valence band are still well separated and the structure distorts, although in a different fashion than in the LnPS series. Going to the higher homologues such as antimonides and tellurides, these differences are "washed out". Similar phenomena can be observed in other cases, e.g., for transition-metal pnictides MX the phosphides occur in the NiAs structure and a variety of distorted versions, whereas the antimonides and bismuthides prefer almost exclusively the high-symmetry NiAs structure.[89,90] The reason is increased overlap between the metalloid and metal band. For LnXY compounds things are a little bit more complicated in that different undistorted structure types evolve for different electron counts: the MAB type for the tellurides, and the $LaSb_2$,[91] $ZrSi_2$,[54] or $CaSb_2$[56] type for the antimonides. The main difference for these structures (except for $EuSb_2$, see below), however, is in the LnX slab of the lattice. Assuming six electrons per atom in the 4^4 net or X–X chains, and a full octet for the isolated Y atoms, we find an oxidation state of 2^+ for the metal atom. An interpretation for these structural changes might be that due to the increased band overlap better stabilization is achieved by a transposition in the LnY slab than by breaking the square net.

We must admit that our calculations cannot explain why almost all actinide compounds occur in the MAB (or in some cases $LaSb_2$) structures. Two examples: Thorium compounds ThXY (X = P, As, Sb; Y = S, Se, Te)[32] are reported to occur in the MAB structure and to be diamagnetic. Assuming a formal oxidation state of 4^+ for Th, there is an odd number of electrons per formula unit. A number of investigations have been performed on U compounds. Taking UAsSe, experimental data suggest a bandgap of ~2 eV between the valence band and the U 6d block,[92] a very narrow 5f band close to the Fermi level, and approximately three electrons localized on uranium,[93] leaving us with U^{3+} and a formally half-filled As band. Mössbauer spectra indicate the presence of tetravalent Np ions in $NpAs_2$;[94] again we would formally get $Np^{4+}As^-As^{3-}$ and the structure would be predicted to distort according to our simple picture.

The $ZrSi_2$ Structure

In the introduction we showed that the $ZrSi_2$ structure can be derived from the ZrSiS (MAB, PbFCl) structure by shifting a ZrS layer of the ZrS slab in the ZrSiS lattice by $a/2$. The essence of this deformation is shown in **34**.

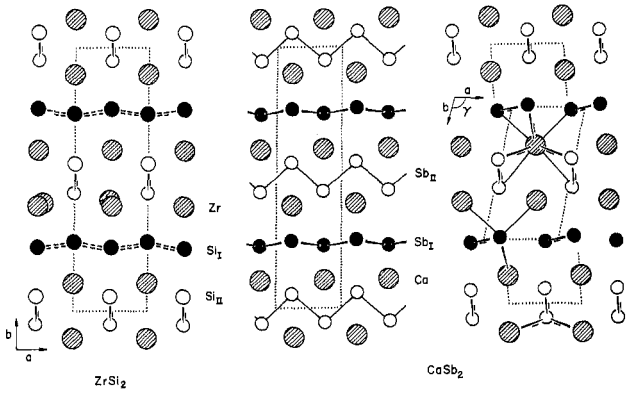

34

$ZrSi_2$ is electron deficient compared to ZrSiS. The material helps itself by forming Si–Si zigzag chains, and the close correspondence can be seen by comparing $[Si_n]^{2n-}$ and S^{2-}. Most of the $LnSb_2$ compounds crystallize in the related $LaSb_2$ structure type,[91] where the LnSb slab contains Sb pairs, but $YbSb_2$ was reported to crystallize in the $ZrSi_2$ structure type.[57] The connection is clear if one remembers that some RE metals such as Sm, Eu, or Yb exhibit di- and trivalent behavior. For Eu and Yb in the divalent state the 4f shell is either half-filled or filled. This leads for Yb to nonmagnetic behavior in the divalent state; in the trivalent state one unpaired 4f electron can generate an effective magnetic moment of 4.5 μ_B, and the statistical number of Yb atoms in the two valence states can easily be measured[57c].

Using our knowledge of the MAB band structure we can guess the relevant part of the $ZrSi_2$ band structure. Since we are interested in the $YbSb_2$–$EuSb_2$ transition, our actual calculations are done on $YbSb_2$. Sure enough, the Sb s bands are lowest in energy. Next come the p bands. The bands of the 4^4 net have an appreciable dispersion and we may expect a crossing of p_x and p_y bands of the square net in the middle of the p block. The p_z bands exhibit only a small band width in the "layers" of the BZ. The B atoms in the MAB structure are isolated, and therefore bands centered on them have only a very small dispersion. Some bands centered on atoms of the zigzag chain in the $ZrSi_2$ structure, however, should exhibit a substantial dispersion in the chain direction. Moreover, the bands should overlap with bands of the square sublattice, whereas they were lower in energy before because of the different electronegativity of Si and S. We expect the Fermi level to lie somewhere in the middle of the p block, possibly close to the band crossing of the 4^4 net. As one can see from the calculated DOS projection in Figure 14, for $ZrSi_2$ the metal d block overlaps the Si p band to some extent and the material should be metallic. In $YbSb_2$ the Yb and Sb bands are well separated.

There is one more point to consider before we proceed to the calculated band structure of $YbSb_2$. Since we are interested eventually in the distortion to the $EuSb_2$ structure or the distortion of the 4^4 net of Sb atoms, we need to think about the appropriate symmetry lines for our calculations. $ZrSi_2$ crystallizes in a C-centered orthorhombic cell (SG: *Cmcm*) and $EuSb_2$ in a primitive monoclinic lattice (SG: $P2_1/m$). Comparing the BZs for both lattices, there is only one common symmetry line ΓZ, because in

(89) For reviews see: Kjekshus, A. *Prog. Solid State Chem.* **1964**, *1*, 83. Hulliger, F. *Struct. Bonding (Berlin)* **1968**, *4*, 83.
(90) Tremel, W.; Hoffmann, R.; Silvestre, J. *J. Am. Chem. Soc.* **1986**, *108*, 5174. Silvestre, J.; Tremel, W.; Hoffmann, R. *J. Less-Common Met.* **1986**, *116*, 113.
(91) Wang, R.; Steinfink, H. *Inorg. Chem.* **1967**, *6*, 1685.
(92) Brunner, H.; Erbudak, M.; Hulliger, F. *Solid State Commun.* **1981**, *38*, 841.
(93) Reim, W.; Schoenes, J.; Hulliger, F. *Physica B* **1985**, *130*, 64.
(94) Boge, M.; Chappert, J.; Asch, L.; Kalvius, G. M.; Blaise, A.; Fournier, J. M.; Damien, D.; Wojakowski, A. *J. Magn. Magn. Mater.* **1982**, *30*, 127. Therond, P. G.; Blaise, A.; Chiapusio, J.; Fournier, J. H.; Wojakowski, A. *J. Less. Common Met.* **1986**, *121*, 227.

(95) See: (a) Klemm, W. *Proc. Chem. Soc. (London)* **1958**, 329. (b) Schäfer, H.; Eisenmann, B.; Müller, W. *Angew. Chem.* **1973**, *85*, 742; *Angew. Chem., Int. Ed. Engl.* **1973**, *12*, 694. (c) Schäfer, H. *Annu. Rev. Mater. Sci.* **1985**, *15*, 1.

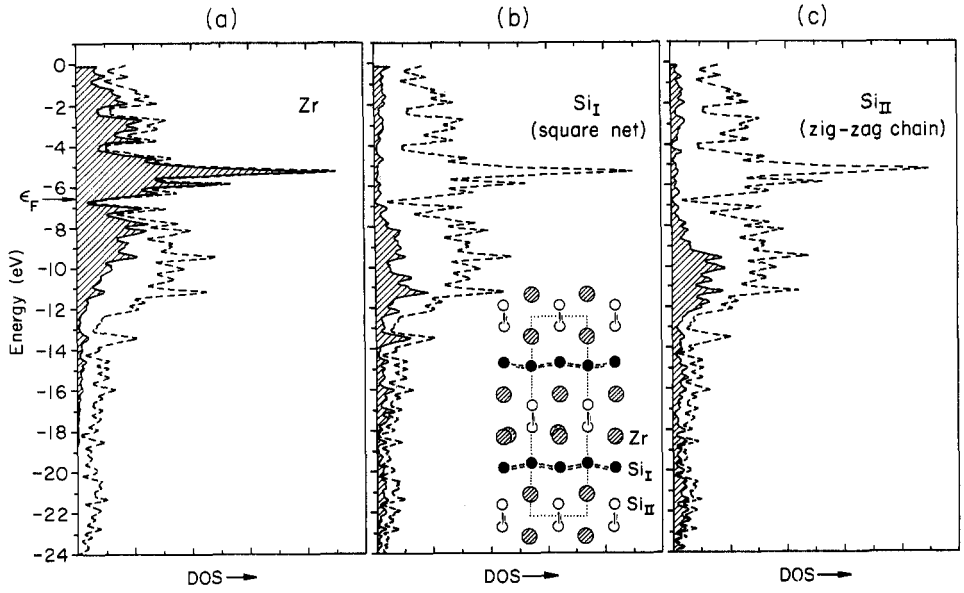

Figure 14. Total DOS (dashed line) and projected DOS (solid line) for $ZrSi_2$ ($ZrSi_2$ structure type) showing (a) metal atom, (b) Si_I atom (placed in the square net), and (c) Si_{II} (placed on the zigzag chain) contributions.

the monoclinic BZ the symmetry is only $2/m$. Taking into account the layer-like character of the materials and the correspondence to the monoclinic cell as given in **5**, **6**, and **35**, Γ–Z is a natural choice.

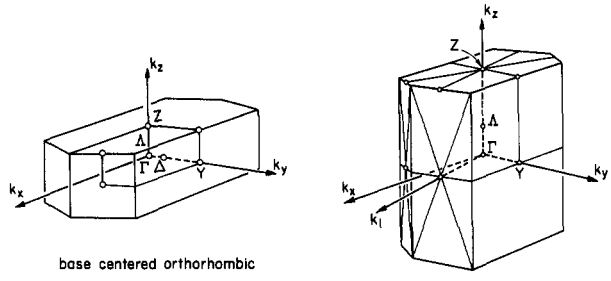

35

The calculated band structure for $YbSb_2$ in the $ZrSi_2$ structure is shown in Figure 15a along the symmetry line Γ–Z. The symmetry along this line is C_{2v} and the symmetry labels refer to the mirror plane and the 2_1 screw axis. In Figure 15a the heavy lines along Γ–Z refer to bands centered mainly on the square net, and the other bands are centered on the zigzag chain. Dashed lines indicate the shape bands would have without mixing. These mixings make things slightly more complicated, but the overall picture is very close to the one we have outlined before. The band structure after the distortion to the $EuSb_2$ structure is given in Figure 15b. The band crossing has disappeared and a bandgap has opened up. The bands that mix strongly are mainly composed of p_x and p_y orbitals of the Sb atoms in the 4^4 net; the orbital mixing mechanism is almost the same as shown in **26**–**29** for the ZrSiS–CeAsS transformation. From the DOS projections (not presented here) we know that the Sb p-contribution is centered in a region of about ±3 eV around the Fermi level. In Figure 16a,b we compare the bonding between atoms within the nets and the chains in the $ZrSi_2$ (a) and $CaSb_2$ (b) structure. The most important features are the following: (i) The dispersion of bands centered on the nets and chains is comparable. (ii) For the undistorted structure the Sb–Sb bonding in the zigzag chain is stronger than in the 4^4 nets (the corresponding antibonding interactions are stronger as well). (iii) The transition between the two structure types does not affect bonding within the chains significantly; the interactions within the 4^4 nets, however, get stronger. (iv) Whereas there is a nonzero DOS at the Fermi level in the $ZrSi_2$ structure, a bandgap opens up for the distorted phase.

Having a good picture of the distortion, the question still to be answered is why $EuSb_2$ distorts but $YbSb_2$ does not. The occurrence of $YbSb_2$ in the $ZrSi_2$ structure implies divalency, but the magnetic data indicate the presence of small amounts (~2%) in the trivalent state as well.[57] Hulliger and Schmelczer[58] therefore suggest that absence of the distortion is triggered by this valence instability. This picture finds support from our calculations. Let us assume $YbSb_2$ has the $ZrSi_2$ structure and Yb is entirely present as Yb^{2+}. This would mean all bands in Figure 15 are filled up to the band crossing close to −11 eV. Some bands are lowered in energy by the distortion, and some bands are pushed up. If only the stabilized levels are filled, as would be the case for purely divalent Eu, the distorted structure would be energetically preferred. If Yb is also present in its trivalent state, the extra electron has to occupy the destabilized levels. If we feed a sufficient number of electrons into these levels or if the levels are pushed up high enough, the undistorted structure will be preferred after a critical electron filling is reached. Apparently this must be the case for $YbSb_2$.

When can we expect materials in the $ZrSi_2$ structure to distort? If the non-metal bands overlap with the metal block, as in $ZrSi_2$, we expect an undistorted structure. If on the other hand metal and non-metal bands are well separated, as in $CaSb_2$,[56] the distorted structure is preferred. This conclusion is exactly Zintl's rule,[95] and the $CaSb_2$ structure can easily be explained with Zintl's ideas. It is for the borderline cases and exceptions such as ZrSiS or $ZrSi_2$ where our calculations aid understanding and become useful. As before we cannot make predictions for the actinide compounds like $ThGe_2$,[53] which again prefer the high-symmetry structure.

Since the binary phases are investigated very well, it is difficult to make any synthetic suggestions. What comes to mind, however, is the possibility of doping Eu into $YbSb_2$ in order to hit the critical electron count at which the distortion occurs. Two things could happen. A continuous transition between the undistorted and distorted phases might be observed, as in the ZrSiS–CeAsS case. The more interesting possibility would be a rapid transition between both phases, as observed in second order phase transitions.[96] In these transitions the structural change—propagated through the crystal like a thermal wave—is very fast and takes place in a very narrow temperature range. Since the transformation is coupled to a metal–semiconductor transition, any material that could undergo this type of transition would have interesting ap-

(96) Franzen, H. F. *Second Order Phase Transitions and the Irreducible Representations of Space Groups*; Springer-Verlag: Berlin, Heidelberg, New York, 1982; Lecture Notes in Chemistry, Vol. 32.

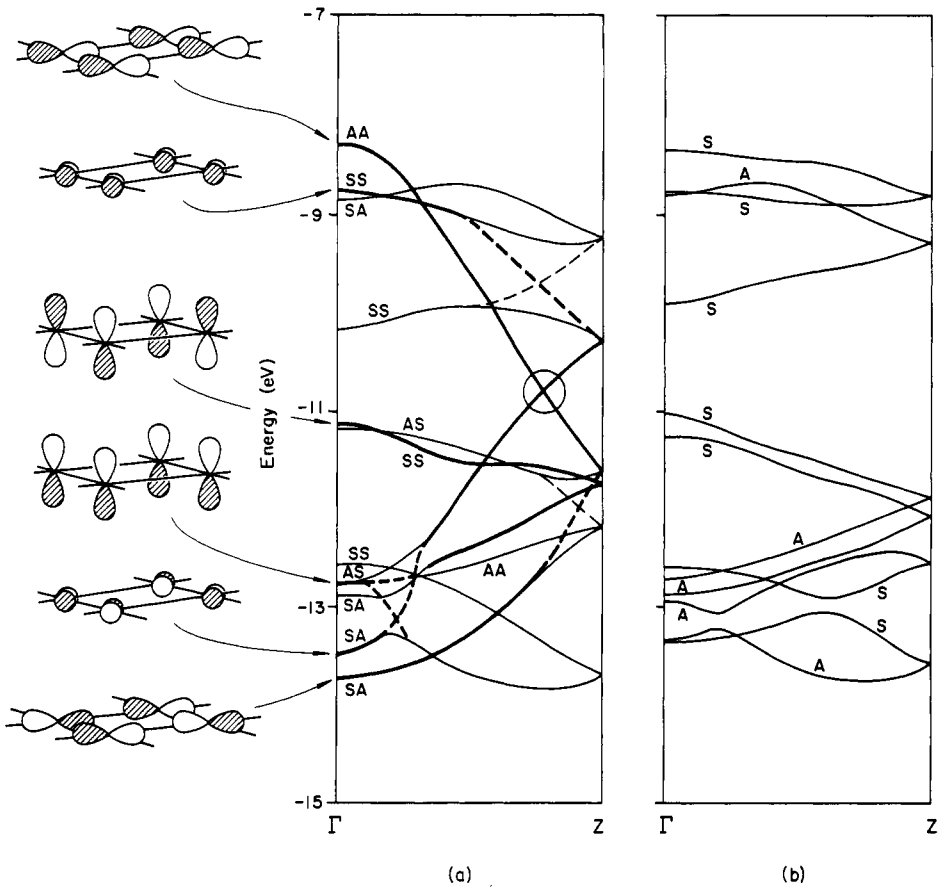

Figure 15. (a) Band structure of $YbSb_2$ in the $ZrSi_2$ structure along Γ–Z. The heavy lines refer to bands centered on the Sb_I (placed on the square net), the other bands are centered on Sb_{II} (placed on the zigzag chain). Dashed lines indicated the shape bands would have without mixing. The symmetry labels refer to the mirror plane and the 2_1 screw axis. (b) Band structure of $YbSb_2$ in the $CaSb_2$ structure along Γ–Z. The symmetry labels refer to the 2_1 screw axis.

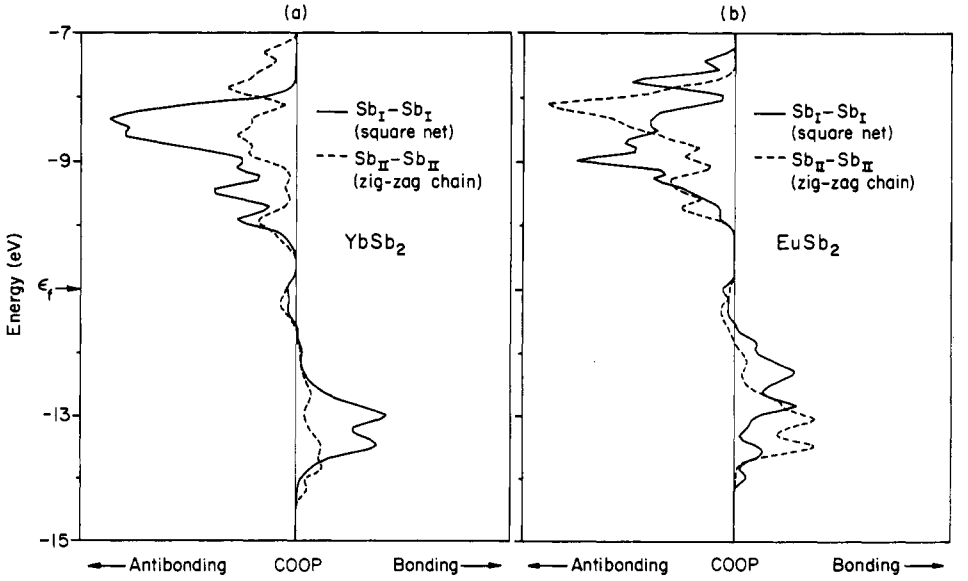

Figure 16. COOP curve for $YbSb_2$ in (a) the $ZrSi_2$ and (b) the $CaSb_2$ structure: (a) dashed line, Sb_I–Sb_I (square net); solid line, Sb_{II}–Sb_{II} (zigzag chain); (b) solid line, Sb_I–Sb_I (square net); dashed line, Sb_{II}–Sb_{II} (zigzag chain).

plications, e.g., in fast temperature-controlled switching devices. The $YbSb_2$–$EuSb_2$ case fulfills the symmetry requirements for a displacive phase transition. There is one further experimental hint that a transition similar to a second order phase transition might exist. Deller and Eisemann[56] reported that crystals of $CaSb_2$ were frequently twinned. This is reminiscent of the famous Dauphiné twins in the α–β quartz transition[97] and indicates a possible high-temperature transition between $ZrSi_2$ and $CaSb_2$ structures. The transition would be coupled to the valence instability in $YbSb_2/EuSb_2$.

(97) Megaw, H. D. *Crystal Structures: A Working Approach*; Saunders Co.; Philadelphia, 1973; p 453.

Deformations in ATB_2 Materials

There is another example we would like to present. From the ternary systems Ca,Sr,Ba(A)/Zn,Cd,Mn(T)/Sb,Bi(B) and La-(A)/Mn,Co,Cu(T)/Sb(B) materials of stoichiometry ATB_2 have been isolated. The bonding in these cannot be simply explained by Zintl's rules.[95] The structure can be derived essentially by

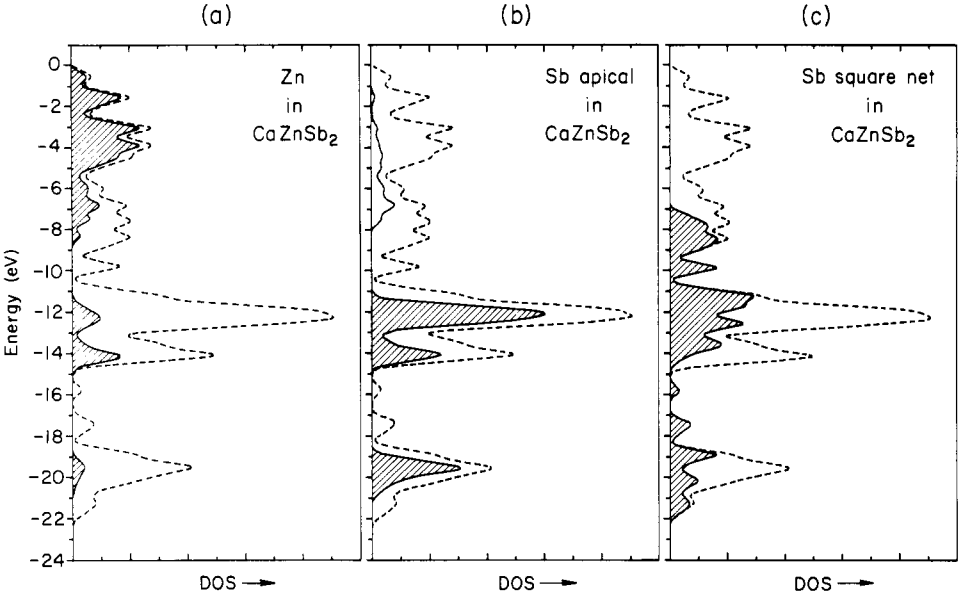

Figure 17. Total DOS (dashed line) and projected DOS (solid line) for $CaZnSb_2$ giving (a) the Zn, (b) the Sb_I, and (c) the Sb_{II} (square net) contributions.

stacking AlB_4-type TB layers and 4^4 nets of Sb and Bi in an AB-like fashion. All of the materials given in Table II except for $SrZnSb_2$ are undistorted, as $SrZnBi_2$ **36**. In $SrZnSb_2$, **37**, the 4^4 net distorts to form now familiar Sb–Sb zigzag chains.

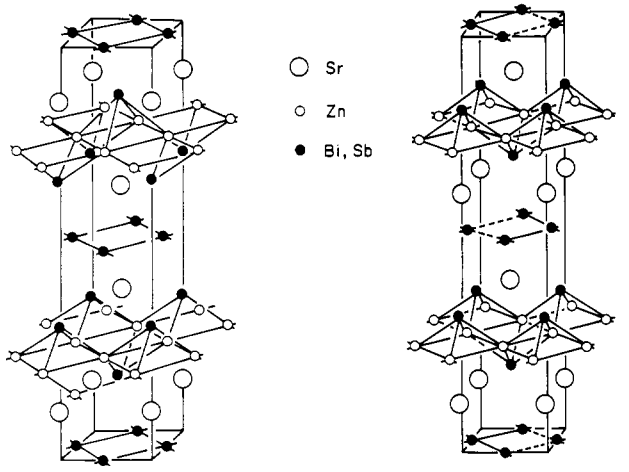

36 **37**

Using the know-how that we have gathered up to this point, we should be able to give a good sketch of the band structure of these materials and to reveal the driving force for the distortion. We can safely neglect the alkaline earth metal and assume because of their low electronegativity that they merely donate electrons to the lower lying bands. Thus we are left with the 4^4 net of Sb atoms and the ZnSb slabs; the two additional electrons are shared between these two fragments. We expect the Zn states to be high in energy and the Sb states low. As a result the Zn atoms give their electrons away and the Sb states are filled.

We can be still more explicit: The Sb atoms of the ZnSb slab form two square nets in the unit cell, which are related by a glide plane. The Zn atoms also form a square net, but now the atoms are twice as dense as before. This net can be regarded as a superposition of two square nets with a topology identical with the 4^4 layer of Sb atoms. We know the band structure for a square net by now. The presence of two square nets related by a glide plane just means that a symmetric and antisymmetric combination of orbitals with respect to the glide plane is formed. As a consequence of the nonsymmorphic symmetry element the bands stick together along the X–M line. The low-lying Sb bands are very

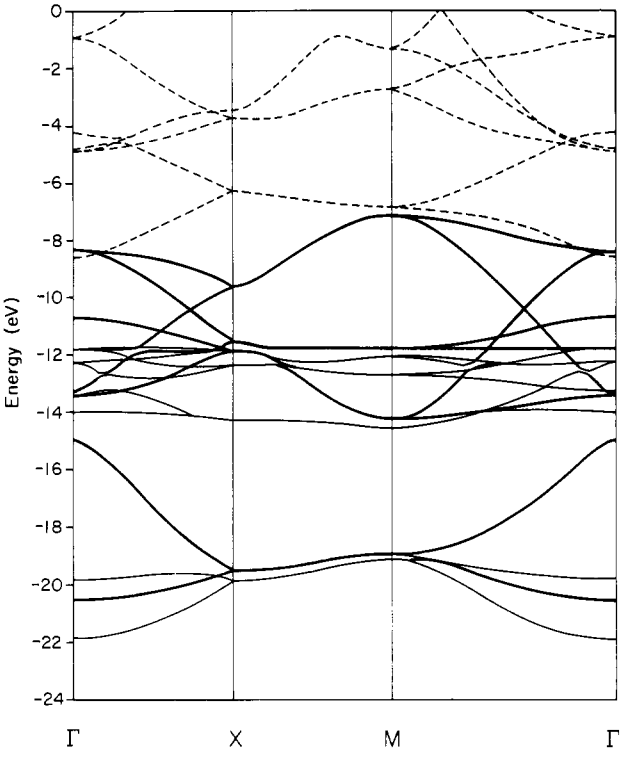

Figure 18. Band structure of $CaZnSb_2$. Bands centered on Sb_{II} (square net) drawn as heavy lines, bands centered on Zn as dashed lines, bands centered on Sb_I (isolated) as normal lines.

narrow because the Sb–Sb distance is large. The Zn–Zn distance is much shorter and therefore the high-lying Zn bands display much more dispersion. Since all the low-lying levels are filled, it is not surprising that the more electropositive atom prefers the more dispersive site.

Thus we can sketch the energy bands of the ZnSb slab as being generated from the bands of four square nets of Zn and Sb atoms. Next we put in the 4^4 Sb net. This net and the ZnSb slab are separated in the real structure by a layer of Ca atoms. There is no direct interaction between both fragments, and the bands of each fragment are in a first approximation only influenced by "electrostatic" interaction with the alkaline earth atoms. Therefore we still get a pretty good picture of the complete band structure if we simply superimpose the two fragment bands. Our qualitative argument is reflected in the DOS projections in Figure 17. States

Table III. Extended Hückel Parameters

orbitals		H_{ii} (eV)	ζ_1	C_1[a]	ζ_2	C_2[a]
Yb	6s	−5.35	1.54			
	6p	−5.35	1.54			
	5d	−5.21	2.810	(0.7063)	1.216	(0.4834)
	4f	−13.86	8.629	(0.7460)	3.198	(0.4564)
Zr	5s	−6.27	1.82			
	5p	−4.11	1.78			
	4d	−6.57	3.840	(0.6226)	1.505	(0.5784)
Zn	4s	−12.41	2.01			
	4p	−6.53	1.70			
Ca	4s	−7.00	1.10			
	4p	−4.00	1.10			
Si	3s	−17.30	1.38			
	3p	−9.20	1.38			
P	3s	−18.60	1.82			
	3p	−14.00	1.82			
Sb	5s	−18.80	2.50			
	5p	−11.70	2.38			
S	3s	−20.00	2.12			
	3p	−13.30	1.83			

[a] Coefficients used in double-ζ expansion

centered on the isolated Sb atoms are localized and states centered on atoms of the square net spread out over the whole valence band. For technical reasons our calculations are done on $CaZnSb_2$ in the $CaMnBi_2$ structure, but the argument remains unchanged. The calculated band structure along selected symmetry lines is shown in Figure 18; the bands centered on the square net are drawn as heavy lines and bands centered on the Zn atoms as dashed lines. The close similarity of the fragment band structures with the energy bands of individual square nets is clearly visible.

Compared to the cases we discussed before, the Sb and Zn bands are very close in energy, and there is even some overlap. The Fermi level for $CaZnSb_2$ is at −10.8 eV. On the basis of our previous experience a red flag goes up if we see the crossing bands close to the Fermi level. The actual orbital picture for the formation of zigzag chain from a square net is the same as given in **26–29**. We can be sure that the incipient overlap of Zn and Sb bands is the reason that most materials in Table II occur in the undistorted structure. Substituting Sb by Bi increases the energy of the valence band and the metal block and the crucial band crossing is buried in the metal bands. In this case there is no stabilization by the distortion, and in fact $AZnBi_2$ compounds prefer the undistorted structure. Substituting Zn by Mn or another 3d metal places the crossing right in the middle of the partially filled metal bands, and it is no surprise that the Mn, Co, and Cu compounds occur in the high-symmetry structure. So the only candidates for a distorted structure are $AZnSb_2$ materials.

The undistorted structure could be encouraged to form again by adding some electrons, e.g., by substituting some Sb by Se or some Ca by La. Any possibility which brings the band crossing closer to partially filled bands stabilizes the undistorted structure. The distorted materials, on the other hand, could be stabilized by lowering the valence band or lifting up the metal bands in energy, or possibly by removing some electrons from the valence band. One possible strategy to lower the valence band in energy might be to replace Sb by As or even P (assuming that we still maintain the general structure type on doing this). One can speculate about quaternary phases where Sb is substituted by Ge and Se. The Ge atom should go into the 4^4 net and the Se atom into the ZnSe slab. The band crossing, however, would probably end up in the metal bands, so as to give an undistorted structure. If there were a way to move up the metal bands high enough, e.g., by replacing Zn by a divalent RE metal, the distorted structure might become stable again.

Acknowledgment. W.T. thanks Ralph Wheeler and Chong Zheng for many discussions and for sharing their expertise with him. Dr. V. Ortiz provided the Yb parameters and a program to calculate the lanthanide exponents and it is a pleasure to thank him for that. The stay of W.T. at Cornell was made possible by fellowships from DAAD/NATO and the Deutsche Forschungsgemeinschaft (DFG). Our research at Cornell was generously supported by the National Science Foundation through research Grant No. DMR-821722 to the Materials Science Center. We are grateful to Kathy Dedrick for the typing and Jane Jorgensen and Elisabeth Fields for their expert drawings.

Appendix

The experimental geometries were used for the GdPS,[48] CeAsS,[49] $ZrSi_2$,[53a] $YbSb_2$,[67b] and $EuSb_2$[58] structures. For the ZrSiS structure the experimentally determined parameters[41] with lattice parameters a = 3.8077 Å, c = 8.371 Å and for $CaZnSb_2$ the experimentally determined parameters of the $CaMnBi_2$[62] structure with lattice parameters a = 4.405 Å, c = 10.847 Å were used.

The Extended Hückel method[69,70] in the tight binding approximation[71] was used in all calculations. The parameters are listed in Table III. For Sb the exponents were contracted to match the experimental DOS[98] and a theoretical band structure,[99] in particular along the line ΓT and at Γ. The Yb parameters were obtained as described in ref 100. Calculations on RE compounds were carried out in part with and without inclusion of 4f orbitals. The results presented were calculated without using 4f orbitals. Sets of 27 or more k points were choosen according to ref 101 to calculate DOS and COOP curves.

(98) Ley, L.; Pollak, R. A.; Kowalczyk, S. P.; McFeely, R.; Shirley, D. A. *Phys. Rev. B* **1973**, *8*, 641.
(99) Bullett, D. W. *Solid State Commun.* **1975**, *17*, 965.
(100) Ortiz, V.; Hoffmann, R. *Inorg. Chem.* **1985**, *24*, 2095.
(101) Pack, J. D.; Monkhorst, H. J. *Phys. Rev. B* **1977**, *16*, 1748.